Anthocyanins act as a sugar-buffer and an alternative electron sink in response to starch depletion during leaf senescence: a case study on a typical anthocyanic tree species, *Acer japonicum*

Mitsutoshi Kitao[1,*], Kenichi Yazaki[1], Hiroyuki Tobita[2], Evgenios Agathokleous[3], Junko Kishimoto[4], Atsushi Takabayashi[4], Ryouichi Tanaka[4]

[1]Hokkaido Research Center, Forestry and Forest Products Research Institute, Hitsujigaoka 7, Sapporo 062-8516, Japan; [2]Department of Plant Ecology, Forestry and Forest Products Research Institute, Matsunosato 1, Tsukuba 305-8687, Japan; [3]Department of Ecology, School of Ecology and Applied Meteorology, Nanjing University of Information Science & Technology (NUIST), Nanjing 210044, China; [4]Institute of Low Temperature Science, Hokkaido University, Kita-19, Nishi-8, Kita-Ku, Sapporo 060-0819, Japan

* corresponding author, e-mail: kitao@ffpri.affrc.go.jp

Date of submission: 27 Feb 2024

Tables: 1, **Figures:** 11, **Word count:** 6218, **Supplementary Tables:** 7, **Supplementary Figures:** 11, **Supplementary Data Table:** 3

Running title

Anthocyanins as a sugar-buffer and an alternative electron sink during autumn senescence

Highlight

Anthocyanins act as a sugar-buffer and an alternative electron sink during leaf senescence after cessation of starch synthesis to prevent sugar-mediated early senescence and photoinhibition.

Abstract

We hypothesized that anthocyanins act as a sugar-buffer and an alternative electron sink during leaf senescence to prevent sugar-mediated early senescence and photoinhibition. To elucidate the anthocyanin role, we monitored seasonal changes in photosynthetic traits, sugar, starch and N contents, pigment composition, and gene expression profiles in leaves exposed to substantially different light conditions within a canopy of an adult tree of fullmoon maple (*Acer japonicum*). Enhancement of starch amylolysis accompanied with cessation of starch synthesis occurred in the same manner independent of light conditions. Leaf sugar contents increased, but reached upper limits in the late stage of leaf senescence, even though leaf anthocyanins further increased after complete depletion of starch. Sun-exposed leaves maintained higher energy consumption via electron flow than shade-grown leaves during leaf N resorption. Thus, anthocyanins accumulated in sun-exposed leaves might have a regulative role as a sugar buffer, retarding leaf senescence, and an indirect photoprotective role as an alternative sink for electron consumption to compensate declines in other metabolic processes such as starch and protein synthesis. In this context, anthocyanins might be key substrates protecting both outer-canopy leaves (against photoinhibition) and inner-canopy leaves (via shading by outer-canopy leaves) from high light stress during N resorption.

Keywords: alternative electron sink, holocanopy hypothesis, N resorption, photoinhibition, starch depletion, sugar-buffer

Introduction

Functions of autumn coloring, involved in red pigments, anthocyanins, have been debated for a long time. Two major hypotheses on the function of autumn coloring have been proposed. According to “photoprotection hypothesis”, anthocyanins act as sunscreen and antioxidants to protect against high light under low temperature, preventing photooxidative stress (Hoch *et al.*, 2001, 2003; Feild *et al.*, 2001; Neill *et al.*, 2002; Renner & Zohner, 2019, 2020; Moustaka *et al.*, 2020). Instead, “co-evolution hypothesis” postulates a function as a signal for insect-tree interaction, where red color appeals high chemical defense investment and low leaf nutrient quality against insects (Archetti *et al.*, 2009; Pena-Novas & Archetti, 2020, 2021; Hughes *et al.*,

2022). Regarding the photoprotection hypothesis, accumulation of anthocyanins contributes to efficient leaf N resorption by preventing photooxidative stress (Hoch *et al.*, 2003; Renner & Zohner, 2019, 2020). However, red leaves with anthocyanins not always showed higher N resorption efficiency than green leaves (Pena-Novas & Archetti, 2020, 2021).

Recently, we also proposed the "holocanopy hypothesis", which posits that outer-canopy leaves protect inner-canopy leaves from photoinhibition by shading, facilitating leaf N resorption in inner-canopy leaves (Kitao *et al.*, 2022). Regarding this hypothesis, prevention from early senescence in the outer-canopy leaves is essential. Furthermore, circumvention of photoinhibition in the outer-canopy leaves *per se* might be necessary for efficient N resorption as a whole canopy because photoinhibition in the middle of leaf senescence causes insufficient N resorption (Hoch *et al.*, 2003; Kitao *et al.*, 2022). To support "holocanopy hypothesis", further investigation of the role of anthocyanins is needed.

Fullmoon maple is a late successional tree species with flush type shoot development, which flushes all leaves once in spring, irrespective of canopy positions (Kikuzawa, 1983; Koike, 1990). Outer-canopy leaves of fullmoon maple turn red earlier, with a higher amount of anthocyanins than inner-canopy leaves during autumn (Koike, 1990, 2004), whereas leaves shed almost simultaneously at any position of the canopy based on field observations (Fig. S1). This implies that leaf senescence of fullmoon maple, including N resorption might be seasonally-programmed irrespective of growth light conditions, possibly responding to photoperiod (Keskitalo *et al.*, 2005). Thus, using leaves grown under different light conditions within the canopy of fullmoon maple, we can distinguish the light-independent processes involved in programmed leaf senescence from the light-dependent protective or regulative processes related to anthocyanin accumulation.

"Photoprotection" is constituted by various processes, including reduction in light absorption, scavenging of reactive oxygen species (ROS), and circumvention and dissipation of excessive light energy, to prevent cellular damage from excessive light energy (Long *et al.*, 1994; Horton *et al.*, 1996). Anthocyanins are considered to have the former two photoprotective roles, attenuating light by screening and acting as antioxidants (Hoch *et al.*, 2001; Neill *et al.*, 2002; Moustaka *et al.*, 2020). Conversely, energy consumption by electron transport mainly involved in photosynthesis and photorespiration (Cornic & Fresneau, 2002; Kitao *et al.*, 2018, 2019) and energy dissipation by non-photochemical quenching might play relevant photoprotective roles

(Ruban, 2016; Murchie & Ruban, 2020). Anthocyanins are glycosides composed of the anthocyanidin aglycone, typically attached to one or more sugar moieties (de Pascual-Teresa & Sanchez-Ballesta, 2008; Wallace & Giusti, 2015), synthesized from photosynthates through the shikimate, general phenylpropanoid, and flavonoid pathways, by consuming further chemical energy such as ATP and NADPH produced by the thylakoid reactions (cf. 2ATP and 4NADPH are required for anthocyanin biosynthesis from erythrose-4-phospate + phosphoenolpyruvate) (Hernández & Van Breusegem, 2010; Soubeyrand *et al.*, 2018). Conversely, excessive ATP and NADPH in grape cell suspensions under N limitation might be the metabolic driver of anthocyanin biosynthesis (Soubeyrand *et al.*, 2018). As anthocyanins are synthesized in the cytosol, chloroplast malate valve and triose phosphate-3-phosphoglycerate shuttle, exporting reducing equivalents and ATP from chloroplast to cytosol, might be involved (Shameer *et al.*, 2019).

Thus, Hernández and Van Breusegem (2010) proposed that the synthesis and accumulation of flavonoids, including anthocyanins and flavonols, can be an alternative sink for photosynthates, which could represent an efficient pathway consuming chemical energy such as ATP and NADPH. Accordingly, anthocyanins might be involved in the photoprotective energy consumption alternative to primary metabolites such as sugars and starch.

Regarding regulation of autumn senescence, leaf sugars are considered as input signals and energy suppliers for leaf senescence (Ono *et al.*, 2001; Wingler *et al.*, 2006; Kim, 2019). During leaf senescence, the level of leaf sugar contents increases with decreasing starch levels (Kim, 2019). As anthocyanins are synthesized from accumulated sugars in leaves during autumn senescence (Stitt & Hurry, 2002; Hughes *et al.*, 2022), anthocyanins could act as a sugar-buffer, preventing early sugar-mediated leaf senescence (Ono *et al.*, 2001; Landi *et al.*, 2015; Lo Piccolo *et al.*, 2018; Lo Piccolo & Landi, 2021; Davies *et al.*, 2022). Among anthocyanins, Cyanidin 3-*O*-glucoside was mainly found in autumn leaves of *Acer palmatum*, a closely-related species to *A. japonicum* (Iwashina & Murai, 2008). Cyanidin 3-*O*-glucoside ($C_{21}H_{21}O_{11}$) has 3.5 times as many C skeletons as glucose ($C_6H_{12}O_6$). Both as an alternative sink for photosynthates and a sugar-buffer, accumulation of anthocyanins is expected to protect outer-canopy leaves from photoinhibition, and prevent sugar-induced early leaf senescence.

We hypothesized that anthocyanins might have light-dependent photoprotective and regulative roles to facilitate seasonally-programmed light-independent processes of leaf

120 senescence, i.e., acting as an alternative electron sink and a sugar-buffer. To test this hypothesis,
121 we clarified which processes depended or not on growth light conditions, including
122 photosynthetic traits, sugar and starch contents, and pigment compositions in leaves grown
123 under substantially different light conditions within a canopy of an adult tree of fullmoon maple
124 (*Acer japonicum*) during autumn leaf senescence. We focus on the seasonal changes in the leaf
125 traits measured in 2021, and similar trends were observed in the previous year, 2020 (shown in
126 Supplementary data).

127

128 **Materials and methods**

129 *Plant materials*

130 We chose an adult tree (height: ≈10 m, age: 50 years old) of fullmoon maple (*Acer japonicum*)
131 grown in the arboretum of Hokkaido Research Center, Forestry and Forest Products Research
132 Institute (43.0°N, 141.4°E; 180 m a.s.l.). We monitored seasonal changes in photosynthetic traits,
133 sugar, starch and N contents, pigment compositions, and gene expression profiles in leaves
134 grown under different canopy positions i.e., different light conditions; 1) south-faced outer
135 canopy (high light condition: HL), 2) north-faced outer canopy (intermediate light condition: IL)
136 and 3) north-faced inner canopy (low light condition: LL). Leaves of fullmoon maple flushed at
137 once in the beginning of May 2021. Photosynthetically active radiation (PAR) was monitored at
138 each canopy position by photo-sensors (S-LIA-M003, Onset Computer Corporation, Bourne, MA,
139 USA) combined with data loggers (H21-USB, Onset Computer Corporation) from summer to
140 autumn in 2021. The averaged daily integrated PAR from 15 July to 8 Nov, 2021 was 18.5, 9.8,
141 and 1.3 mol m^{-2} day^{-1} for HL, IL, and LL leaves, respectively (Fig. S2A). Air temperature at a height
142 of 50 cm above the ground was monitored by a thermo-sensor (S-THB-M002, Onset Computer
143 Corporation) placed in a solar radiation shield (RS3, Onset Computer Corporation), beneath the
144 canopy, combined with a data logger (H21-USB, Onset Computer Corporation) (Fig. S2B).

145

146 *Gas exchange and chlorophyll fluorescence measurements*

147 Area-based net photosynthetic rate (A_{area}) and electron transport rate (ETR_{area}) were periodically
148 measured, totally 8 times from summer (29 July) to autumn (25 Oct), in 4 leaves at each canopy
149 position with a portable photosynthesis system (Li-Cor 6800, Li-Cor, Lincoln, NE, USA) combined

with a leaf chamber fluorometer (LI-6800-01A, Li-Cor). Measurements were conducted at an ambient CO_2 concentration of 400 µmol mol^{-1}, a photon flux density (PFD) of 1000 µmol m^{-2} s^{-1}, and a leaf temperature of 20 to 25 °C. To monitor the seasonal change in photosynthetic capacity, we measured A_{area} and ETR_{area} under saturating light (1000 µmol m^{-2} s^{-1}) and optimal leaf temperatures (20 to 25 °C). After the leaves reached a photosynthetic steady state under saturating light (1000 µmol m^{-2} s^{-1}), steady state fluorescence (F_s) and maximum fluorescence under light (F_m') were determined with multi-phase flash method. Quantum yield of photosystem II electron transport (YII, = (F_m'-F_s)/F_m') was also calculated (Genty *et al.*, 1989; Hendrickson *et al.*, 2004; Klughammer & Schreiber, 2008). Leaf absorptance (ABS) was measured with a leaf spectrometer (CI-710, CID Bio-Science, Camas, WA, USA). Leaf absorptance used for the calculation of ETR is generally derived as to photosynthetic active PFD with wavelength ranging from 400 to 700 nm ($ABS_{400-700}$). However, the light source used for the measurements of photosynthetic gas exchange and chlorophyll fluorescence was supplied by an array of red LEDs peaked at 625 nm and an array of blue LEDs peaked at 475 nm equipped with a leaf chamber fluorometer (LI-6800-01A, Li-Cor). A PFD of 1000 µmol m^{-2} s^{-1} for the measurements consisted of 900 µmol m^{-2} s^{-1} of red light and 100 µmol m^{-2} s^{-1} of blue light. Here, we calculated LED-specific leaf absorptance (A_{LED}) by using absorptance at the wavelength of 625 (ABS_{625}) and 475 nm (ABS_{475}) as: A_{LED} = 0.9 ABS_{625} + 0.1 ABS_{475}, then calculated ETR as: ETR = ABS_{LED} x PFD x 0.5 x YII (Demmig-Adams *et al.*, 1996). As the light source consisted of 90% red and 10% blue, the effects of anthocyanins, which absorb some of the 475 nm blue light, are bypassed. Dry mass-based net photosynthetic rate (A_{mass}) and ETR (ETR_{mass}) were also derived by using leaf mass per area (LMA), as described below.

F_v/F_m, = (F_m-F_o)/F_m was measured after an overnight dark-adaptation with a portable chlorophyll fluorometer (Mini-PAMII, Walz, Effeltrich, Germany). F_m is the maximum fluorescence level elicited by a pulse of saturating light (≈ 6000 µmol m^{-2} s^{-1}), and F_o is the minimum fluorescence level. Leaf clips for dark-adaptation (DLC-8, Walz) were attached to the leaves in the evening of the day before the F_v/F_m measurements (i.e., the evening of the day of A_{area} and ETR_{area} measurements). We measured F_v/F_m in the next morning, after overnight dark-adaptation. As F_v/F_m has recently been shown not to be the efficiency of PSII photochemistry (Sipka et al. 2021), we considered F_v/F_m as an empirical measure of PSII activity. Furthermore, as protein carbonylation, a biomarker of oxidative stress by ROS (Anjum *et al.*, 2015), was related to a decrease in F_v/F_m during leaf senescence of *A. japonicum* in a previous study (Kitao *et al.*,

2022), lower F_v/F_m was considered an empirical indicator of photoinhibition in the present study.

Leaf sugar, starch, nitrogen and pigments contents

Leaves used for F_v/F_m were sampled immediately after the measurements. Two thirds of a whole leaf were frozen with liquid nitrogen and stored at −80 °C until further analyses of leaf pigments and gene expression profiles. The other third was sampled for determination of leaf sugar, starch, and N contents. Leaf samples for sugar, starch, and N analyses were dried at 70 °C to constant weight in an electric oven. Leaf area and fresh weight (FW) were measured before drying. Based on leaf area (measured before drying) and dry weight (DW), LMA was calculated. The ratio of DW to FW (DW/FW) was used for converting fresh weight-based values (leaf pigments) to dry mass-based ones. LMA was used for converting dry mass-based values to area-based ones, and vice versa. Details of leaf sugars and starch determination are described in (Kitao *et al.*, 2022). Leaf pigments (anthocyanins, chlorophyll a, b, violaxanthin, antheraxanthin, and zeaxanthin) were determined using the frozen samples. Details of pigment analyses are described in (Kitao *et al.*, 2022).

Isolation of RNA

The leaves harvested at IL and LL on 7 Sep, 28 Sep, 5 Oct and 13 Oct, respectively, were frozen and ground into powder using a Multi Beads Shocker homogenizer (Yasui Kikai Corporation, Osaka, Japan) under liquid nitrogen. Subsequently, total RNA was isolated from 20 mg of powder using ISOSPIN Plant RNA Kit with Assist Buffer (Nippon Gene Co., Ltd., Tokyo, Japan) according to the manufacturer's protocol. The extracted RNA was further purified using the RNeasy PowerClean Pro CleanUp Kit (QIAGEN, Hilden, Germany) according to the manufacturer's protocol. The purification procedure was repeated twice for the RNA samples from 13 Oct leaves, as they appeared to contain excessive sugars after the first purification step. We also attempted to isolate RNA from the leaves harvested on 19 Oct or later, but the yield and the quality of these RNA samples were too low for the subsequent analysis with a next-generation sequencer (data not shown). It was probably because senescence-induced degradation of RNA might have already progressed to some extent on 19 Oct.

Isoform sequencing analysis

To construct the gene models of *A. japonicum,* we performed isoform sequencing (Iso-Seq) analysis with RNA extracted from the leaves in both IL and LL conditions harvested on 7 Jul and 7 Sep in 2021. We chose these leaves before autumn leaf senescence for Iso-Seq, because we expected that these leaves were active in most metabolic pathways so that most genes for the major metabolic pathways were expressed. Details in Iso-Seq analysis, and estimation of full-length protein sequences are shown in Supporting Information (Methods S1,2), and Suppl. Data Table 1.

Gene expression analysis using RNA-seq data

The same set of RNA samples used for the Iso-Seq analysis described above was analyzed with DNBSEQ (MGI Tech Co. Ltd, Shenzhen, China) to yield paired-end 150 bp reads. The fastP program ver. 0.20.0 (Chen *et al.*, 2018) with default settings for paired-end reads was used to clean the RNA-seq reads. Subsequently, the Salmon program ver. 1.9.0 (Patro *et al.*, 2017) was used to quantify the expression of the transcripts using the cleaned reads. The protein-coding regions of the cDNAs obtained from the Iso-seq analysis were used as target sequences for the quantification. Transcripts per million (TPM) calculated by Salmon were used to normalize transcript read counts. The RNA-Seq data have been deposited at DDBJ (DRA016400).

Principal component analysis (PCA) was performed with iDEP (ver. 0.96) (Ge *et al.*, 2018), in which the first and second components point to the direction with the greatest and the second greatest variation among samples, respectively. k-means clustering was also performed with iDEP, in which 1,000 highly expressed genes were selected and grouped into four clusters based on their expression profiles. Results of PCA and k-means clustering are shown in Supplementary data (Fig. S3&S4, Table S1, Suppl. Data Table 2).

Functional annotation of genes

For the Kyoto Encyclopedia of Genes and Genomes (KEGG release 105.0) pathway analysis, the KO identifier of each gene was assigned by KofamKOALA ver.2023-01-01 (Aramaki *et al.*, 2020). In addition, the closest *Arabidopsis* homologue of each gene was searched in the TAIR10

241 database using NCBI-BLASTP (Altschul *et al.*, 1990). The annotations of the KEGG pathway and
242 the closest *Arabidopsis* homologs are summarized in Suppl. Data Table 1.

243 *Acer* genes encoding enzymes involved in carotenoid biosynthesis, tetrapyrrole
244 biosynthesis, sugar and starch metabolism, and flavonoid metabolism were selected by their
245 sequence homology to their *Arabidopsis* counterparts, as most of these *Arabidopsis* genes were
246 shown to encode functional enzymes according to the reference database of the *Arabidopsis*
247 Biological Resource Center (https://abrc.osu.edu).

248

249 *Statistical analysis*

250 Tukey-Kramer multiple comparison test was employed to investigate the differences among the
251 growth light conditions (HL, IL, and LL) in photosynthetic traits, leaf N, sugar and starch contents,
252 and leaf pigment contents on each date (R Core Team & R Development Core Team, 2020), as
253 well as the differences among dates in each light condition (HL, IL, or LL). Regarding F_v/F_m, a
254 stepwise method for variable selection for multiple regression analysis was used for quantitative
255 evaluation of the influence of the explanatory factors (initial variables: integrated solar radiation
256 (PAR_{int}), daily mean temperature, light-saturated net photosynthetic rate (A_{mass} and A_{area}), pool
257 size of xanthophyll cycle (V+A+Z), leaf anthocyanin content) on F_v/F_m. Stepwise regressions were
258 used to define the subset of effects that would altogether provide the smallest corrected Akaike
259 information criterion (AIC) in subsequent modeling. The analysis was conducted for both dry
260 mass- and area-based variables, where area-based $PAR_{int,area}$ was converted to dry mass-based
261 $PAR_{int.mass}$ using LMA to align the units ($PAR_{int,mass} = PAR_{int,area}/LMA$). The level of significance was
262 0.05 with two-tailed testing. In the present study, both dry mass- and area-based variables are
263 shown.

264

265 **Results**

266 *Leaf anthocyanin content, leaf N content, and F_v/F_m*

267 All leaves grown in the canopy of an adult tree of fullmoon maple flushed at the beginning of
268 May 2021, and shed at the beginning of November. We considered that dry-mass based analyses
269 were suitable for seasonal changes in leaf physiological traits, while area-based analyses would

be better to investigate light-dependent processes in response to incident light, generally expressed on the basis of area. Leaf anthocyanin contents on the basis of both dry mass ($Anthocyanin_{mass}$) and leaf area ($Anthocyanin_{area}$) started to increase gradually from early October in all light conditions (Fig. 1A,C). Then, $Anthocyanin_{mass}$ increased 3.3-, 2.2-, and 1.4-fold in HL, IL, and LL leaves from 19 to 29 Oct, while $Anthocyanin_{area}$ increased 2.4-, 2.1-, and 1.2-fold in HL, IL, and LL leaves, respectively (Table S2). Higher LMA was observed in leaves grown under higher PAR (HL > IL > LL) (Fig. S5, Table S3), which caused differences between values on the basis of dry mass and leaf area. Among light conditions, significantly higher $Anthocyanin_{mass}$ was observed in HL and IL leaves than in LL leaves on 21, 26 and 29 Oct (Table S2). Dry mass- and area-based leaf N contents gradually decreased in HL and IL leaves from 28 Sep to 19 Oct, and progressively declined within 10 days toward the end of October (Fig. 1B,D, Table S2). Conversely, Leaf N content in LL leaves was relatively stable throughout the season up to 19 Oct, and then abruptly declined toward the end of October, similarly to the declines observed in HL and IL leaves. It should be noted that most of resorbable leaf N was exported within a week, from 19 to 26 Oct, in all leaves irrespective of growth light conditions. F_v/F_m in all leaves (HL, IL and LL) was relatively stable until 22 Oct, and then significantly declined on 26 Oct (Fig. 1E, Table S2). F_v/F_m was relatively higher in LL leaves than in HL leaves, whereas no significant difference was observed among HL, IL, and LL leaves on 26 Oct, when F_v/F_m declined (Table S2). LED-specific leaf absorptance (ABS_{LED}) was stable with no significant difference among HL, IL, and LL leaves from 17 Aug to 19 Oct, and then declined towards the end of Oct with a higher decreasing rate in LL > IL > HL (Fig. 1F, Table S2).

Leaf chlorophyll and xanthophyll pigments

Both dry mass- and area-based total leaf chlorophyll contents ($Chl_{a+b,mass}$, and $Chl_{a+b,area}$) decreased gradually from summer (27 July) to autumn (19 Oct) in all leaves grown under different light conditions (HL, IL, and LL), and then abruptly declined in all leaves until 26 Oct (Fig. 2A,C, Table S4). The ratio of chlorophyll a to b ($Chl_{a:b}$) in HL leaves was stable throughout the season, while $Chl_{a:b}$ in IL and LL leaves showed significantly higher values on 26 Oct than on other dates (Fig. 2E). Xanthophyll cycle pool size (V+A+Z, sum of xanthophyll pigments; V: violaxanthin, A: antheraxanthin, Z: zeaxanthin) decreased gradually from summer (27 July) to autumn (19 Oct) in all leaves grown under different light conditions (HL, IL, and LL) on the basis of both dry mass

and area (Fig. 2B,D). Although V+A+Z declined substantially from 19 to 26 Oct in IL and LL leaves, that in HL leaves kept a relatively high value even on 26 Oct before minimize in the end of October. The conversion state of xanthophyll cycle [(Z+A)/(V+A+Z)] was generally higher in HL leaves than in IL and LL leaves throughout the season (Fig. 2F). In some cases (17 Aug, 7 Sep, 5 Oct, 19 Oct, and 22 Oct), (Z+A)/(V+A+Z) in IL leaves was higher than in LL leaves (Table S4). Considering mean PAR during 1 h before leaf sampling (Fig. S6), (Z+A)/(V+A+Z) appeared to be light-dependent, where higher (Z+A)/(V+A+Z) was observed under higher PAR across leaves grown under different light conditions from 27 Jul to 12 Oct. Conversely, HL leaves kept high values of (Z+A)/(V+A+Z) even under relatively low PAR from 19 to 26 Oct, while (Z+A)/(V+A+Z) in IL and LL leaves showed increasing trends during leaf senescence from 19 to 26 Oct with relatively constant PAR (Fig. 2F, Fig. S6).

Leaf sugar and starch contents

Dry mass-based leaf sugar content ($Sugar_{mass}$) increased toward autumn, and the highest leaf sugar contents were observed on 22 Oct for HL and IL leaves and on 26 Oct for LL leaves (Fig. 3A, Table S5). Conversely, no significant seasonal changes in area-based leaf sugar content ($Sugar_{area}$) were observed in IL and LL leaves, while an apparent peak of $Sugar_{area}$ was observed in HL leaves on 22 Oct (Fig. 3C, Table S5). Dry mass-based leaf starch content ($Starch_{mass}$) and area-based leaf starch content ($Starch_{area}$) showed similar trends throughout the season (Fig. 3B,D, Table S5). Highest leaf starch contents ($Starch_{mass}$ and $Starch_{area}$) were observed on 17 Aug in HL and IL leaves. Then, $Starch_{mass}$ and $Starch_{area}$ decreased toward the end of October, reaching almost 0. Starch content ($Starch_{mass}$ and $Starch_{area}$) in LL leaves declined from 17 Aug toward the end of October. It is noteworthy that Sugar/(Sugar+Starch) showed no significant difference among the light conditions throughout the season (except for 22 Oct, but the difference was small: 0.96, 0.97, and 0.98 for HL, IL, and LL leaves respectively) (Fig. 3E, Table S5). Sugar/(Sugar+Starch) temporarily dropped on 17 Aug, and then increased from the end of September toward the end of October to reach almost 1 across all light conditions.

Photosynthetic rate and electron transport rate

Mass-based net photosynthetic rate under saturating light (A_{mass}) was relatively stable with no

significant difference among HL, IL, and LL leaves from 26 July to 4 Oct. Then, decreases in A_{mass} were observed from 12 Oct in IL and LL leaves when compared the maximum value in the summertime (26 Jul), whereas A_{mass} in HL leaves declined from 18 Oct while the maximum value was observed on 12 Oct (Fig. 4A, Table S6). Higher A_{mass} was observed in HL than in IL and LL leaves on 12 Oct, while higher A_{mass} was observed in HL leaves than in IL leaves on 18 and 25 Oct. Area-based net photosynthetic rate under saturating light (A_{area}) in HL leaves was stable from 26 Jul to 12 Oct, and then declined toward 26 Oct (Fig. 4C, Table S6). Decline in A_{area} from the maximum value in the summertime (26 July) was observed from 4 Oct in IL leaves, but from 12 Oct in LL leaves. A_{area} was higher in HL and IL leaves than in LL leaves from 26 July to 27 Sep. Thereafter, A_{area} was higher in HL leaves than in IL and LL leaves.

Mass-based light-saturated electron transport rate (ETR_{mass}) showed significant decreases from 26 July to 16 Aug in HL and IL leaves (Fig. 4B, Table S6). Afterwards, ETR_{mass} in HL and IL leaves was relatively stable from 16 Aug to 12 Oct, then declined towards 25 Oct. Conversely, ETR_{mass} in LL leaves decreased gradually from 26 Jul to 12 Oct, and then declined towards 25 Oct. Generally, ETR_{mass} in HL leaves was higher than that in LL leaves throughout the season, and also higher than those in IL leaves around the end of leaf senescence (18 and 25 Oct). Area-based ETR (ETR_{area}) showed similar seasonal changes in HL, IL and LL leaves, whereas generally higher ETR_{area} was observed in leaves grown under higher light intensity (HL > IL > LL) from 16 Aug to 18 Oct (Fig. 4D, Table S6). Significantly higher ETR_{area} was observed in HL leaves than in IL and LL leaves on 25 Oct.

Multiple regression analysis for F_v/F_m

Best model, based on the smallest AIC, included three explanatory variables, namely $PAR_{int,mass}$, A_{mass}, and $Anthocyanin_{mass}$, which significantly predicted F_v/F_m ($F_{(3, 92)} = 86.9$, $p < 0.001$, $r^2 = 0.729$). The coefficients of the three variables were significant ($p < 0.001$), and A_{mass} had a positive coefficient while $PAR_{int,mass}$ and $Anthocyanin_{mass}$ had negative coefficients (Table 1). In addition, a multiple regression to predict F_v/F_m, using area-based variables for $PAR_{int,area}$ A_{area}, $V+A+Z_{area}$, and $Anthocyanin_{area}$, showed a similar result, where A_{area} had a positive coefficient and $PAR_{int,area}$ and $Anthocyanin_{area}$ had negative coefficients to predict F_v/F_m (Table 1).

Relationship between leaf anthocyanins and sugar contents

As described above, [Sugar/(Sugar+Starch)] increased to almost 1 (above 0.90 from 19 Oct) during autumn senescence (cf. Fig. 3E). Leaf anthocyanin contents in IL and HL leaves showed progressive increases when Sugar/(Sugar+Starch) exceeded 0.9, whereas such a progressive increase was not observed in LL leaves (Fig. 5A). Based on the relationship between leaf anthocyanin contents and leaf sugar contents (Fig. 5B, Fig. S7), all leaves (HL, IL, and LL) showed increasing trends in leaf sugar with increasing leaf anthocyanin in leaves sampled from 27 Jul to 19 Oct before progressive leaf N resorption (cf. Fig. 1), whereas leaf sugar contents were almost stable from 22 to 29 Oct during leaf N resorption even when leaf anthocyanin increased. Similar trends were observed in IL and LL leaves measured in the previous year, 2020 (Fig. S8).

Expression profiles of the flavonoid biosynthesis genes

Thirteen genes involved in flavonoid biosynthesis were detected in our Iso-Seq analysis (Suppl. Data Table 3), based on their homology to *Arabidopsis* flavonoid biosynthesis genes (Saito *et al.*, 2013). Among them, ten genes whose expression was higher than their isoforms were selected, and their expression profiles were plotted in Fig 6. Interestingly, all the analyzed genes leading to cyanidin formation showed synchronized expression profiles (Fig. 6). In LL, these genes showed a peak in their expression on 27 Sep, and then decreased. These profiles are consistent with the changes in the anthocyanin levels, which started to increase at the end of Sep (see the insets of Fig. 1A). In IL, the expression of the genes involved in cyanidin synthesis was constant or slightly decreasing until the beginning of Oct, and increased on 13 Oct (Fig. 6). These patterns well explain the changes in anthocyanin contents under IL, which increased till the end of Sep, but decreased once in early Oct, and showed another increase in the mid Oct.

Three F3GlcT genes showed similar expression profiles to each other (Fig. 6). They showed two peaks on 27 Sep and 13 Oct under LL, while they showed a decrease on 27 Sep and an increase in Oct under IL. An increasing trend of the gene expression in Oct is correlated with the onset of anthocyanin accumulation (Fig. 1A). An increasing expression of F3GlcT may indicate that the level of glycosylated anthocyanin increased on and after 13 Oct. UGT84A1 is a UDP-glucosyltransferase family protein having 1-O-glucosyltransferase activity for phenylpropanoids such as p-coumaric acid (Lim *et al.*, 2001). The expression of this gene

391 increased on 27 Sep under IL conditions, otherwise, it was stable at least until 13 Oct.

392

393 *Chlorophyll metabolism*

394 The expressions of three key enzymes of chlorophyll biosynthesis, which include glutamyl-tRNA
395 reductase (HEMA1), the H subunit of Mg-chelatase (CHLH) and Mg-protoIX monomethylester
396 cyclase (MgCy-CHL27), were higher under IL than under LL conditions (Fig. 7). They tended to
397 decrease under LL during developmental senescence, while they were relatively stable until
398 early Oct and showed a decrease on 13 Oct under IL. The expression of the other enzymes in the
399 chlorophyll *a* biosynthesis pathway, including glutamate-1-semialdehyde mutase (GSA), 5-
400 aminolevulinate dehydratase (ALAD), protoporphyrinogen IX oxidase (PPO), and two subunits of
401 Mg-chelatase (CHLD and CHLI), were constant and were synchronized under IL and LL conditions.
402 It is likely that the expressions of these genes are kept high so that none of these enzymes would
403 form a bottleneck in chlorophyll biosynthesis.

404 We detected five genes encoding the enzymes in chlorophyll breakdown in our Iso-
405 Seq/RNA-Seq analysis (Fig. 7), among which the expressions of isoforms of chlorophyll *b*
406 reductase (NYC1), magnesium dechelatase (Stay-Green or SGR), pheophytinase (PPH), and
407 pheophorbide *a* oxygenase (PAO) gradually increased until 5 Oct, and then showed marked
408 increases on 13 Oct, while that of 7-hydroxymethyl chlorophyll *a* reductase (HCAR) was stable.
409 NYC1 is rate-limiting in the chlorophyll *a*-to-*b* conversion, while HCAR is usually abundant and
410 stable (Tanaka & Tanaka, 2011). Therefore, it would be reasonable that the gene expression of
411 HCAR did not show important changes during development.

412

413 *Carotenoid biosynthesis*

414 The expressions of the nine genes encoding enzymes involved in carotenoid biosynthesis were
415 analyzed by RNA-Seq (Fig. 8). Gene expression of the four genes (PSY, PDS, ZDS and CRTISO) for
416 the formation of lycopene were stable and did not even show a decrease on 13 Oct when
417 chlorophyll breakdown started. The genes for two isoforms of zeaxanthin epoxidase (ZEP) and
418 that for violaxanthin deepoxidase (VDE), both of which are involved in the xanthophyll cycle,
419 were stably expressed until 13 Oct. Gene expression for neoxanthin synthase (NSY) increased on
420 13 Oct. Since neoxanthin is a precursor of abscisic acid (ABA), it is possible that a demand for

ABA biosynthesis led to an increase in NSY expression. Gene expression of lycopene ε-cyclase also increased on 13 Oct. It was notable that gene expression for most of the detected carotenoid biosynthesis genes was synchronized under IL and LL conditions.

Sugar/Starch metabolism

Gene expression for the key enzymes of the Calvin cycle, namely the small and the large subunit of Rubisco (RbcS and RbcL), plastid fructose 1,6-bisphosphatase (FBPase) and phoshphoribulokinase (PRK), was stable until 13 Oct. These results indicate that the Calvin cycle was fully active until mid-Oct. Starch biosynthesis is finely controlled by the activity of ADP-glucose pyrophosphorylase (AGPase) (Streb & Zeeman, 2012). Gene expression for the small subunit of AGPase and the second isoform of the large subunit of AGPase gradually decreased in the period between 7 Sep and 13 Oct (Fig. 9A). Among seven genes that encode plastid-localized starch degradation enzymes, those for glucan water dikinase 1 (GWD1), phosphoglucan phosphatase (starch excess 4: SEX4), beta-amylase isoforms 3 (BAM3) and 9 (BAM9) increased, while those for phosphoglucan water dikinase (PWD), isoamylase (ISA) and disproportionating enzyme 1 (DEP1) were stable (Fig. 9B). GWD, SEX4 and BAM are key enzymes in the control of starch degradation (Lu & Sharkey, 2006). Overall, there is a trend toward a gradual increase in gene expression for key enzymes in starch degradation, while gene expression for other enzymes remained at a relatively constant level.

In the cytosol, disproportionating enzyme (D-enzyme, DPE2) and sucrose phosphate synthase (SPS) increased over the course of RNA-Seq analysis (Fig 9B). DPE2 plays an essential role in starch degradation through maltose metabolism (Lu & Sharkey, 2006), while sucrose-phosphate synthase plays a major role in sucrose synthesis (Huber & Huber, 1996) catalyzing the formation of sucrose-6-phosphate. On the contrary, the genes encoding the other enzymes involved in sucrose synthesis show stable expression.

Key regulators in leaf senescence

Trehalose-6-phosphate is known as a regulator of leaf senescence, whose level is correlated with the onset of leaf senescence (Wingler *et al.*, 2012). It is also known to regulate starch degradation and sucrose synthesis (Lunn *et al.*, 2014). In our Iso-Seq and RNA-Seq analysis, we

detected six homologs that putatively encode trehalose-6-phosphate synthase (TPS), while 11 TPS genes have been identified in *A. thaliana*. In *A. japonicum,* four TPS homologs showed relatively stable expression (Fig. 10), while TPS9 and TPS10 showed a sudden increase on Oct 13, a pattern similar to those of key chlorophyll breakdown genes (SGR1, PPH, and PAO in Fig. 7). Even though the roles of TPS genes in the leaf senescence of *A. japonicum* have not been identified*,* it is tempting to speculate that TPS9 and/or TPS10 are involved in the regulation of leaf senescence and sucrose synthesis in *A. japonicum.* It should be noted that we could not detect the transcriptomes for SnRK1, which is a central regulator of energy metabolism whose activity is regulated by trehalose-6-phosphate (Wurzinger *et al.*, 2018).

TOR is a protein kinase involved in various developmental controls by interacting with RAPTOR and LST1 (Henriques *et al.*, 2022). The *TOR* and *RAPTOR* genes showed stable expression patterns during autumn senescence, while the *LST1* gene was not detected in our Iso-seq analysis. Hexokinase is an intracellular sugar sensor involved in developmental control (Kim, 2019). The *HXK2* gene encoding a cytosolic form of hexokinase also showed a stable expression pattern (Fig. 10). It is unclear whether these regulators play a major role in the control of sugar metabolism during autumn senescence in *A. japonicum*.

We also analyzed the expression of a representative senescence marker, SAG12, which encodes vacuolar protease, whose expression increases with leaf senescence (Lohman *et al.*, 1994). Its expression steadily increased during the period of our analysis (Fig. 10). Its expression levels were similar between IL and LL conditions, indicating again that developmental leaf senescence synchronized within the single tree regardless of light conditions.

Discussion

Seasonal changes related to leaf physiological traits could be separated into processes independent or dependent on light, by using a flush type leaf development species, *A. japonicum*. We considered that light-independent would be essential processes related to efficient N resorption during leaf senescence, whereas light-dependent might be protective or regulative processes for the light-independent processes. Here, the seasonal changes in leaf N, F_v/F_m and Sugar/(Sugar + Starch) might be fundamental, and seasonally-programmed independent of light

conditions, primarily responding to photoperiod (Keskitalo *et al.*, 2005; Fracheboud *et al.*, 2009), while photosynthetic activities and leaf pigments (including anthocyanins) might have protective or regulative roles in response to growth light conditions. Similar trends were observed in seasonal changes in IL and LL leaves measured in the previous year, 2020 (Fig. S9).

It was rather surprising that the gene expression for chlorophyll biosynthesis, carotenoid biosynthesis, starch/sugar metabolism, and developmental regulators are synchronized under LL and IL conditions, though the levels of chlorophyll (Fig. 2), xanthophyll cycle pigments (Fig. 2), and starch/sugar showed clear differences between these two conditions. These results may indicate that the final metabolite levels are determined by post-transcriptional regulation including translational controls, modification of enzyme activities, and/or the control of enzyme stabilities via environmental conditions. Anthocyanin biosynthesis is exceptional in this aspect. Expression patterns of genes involved in anthocyanin biosynthesis differed between LL and IL conditions and were correlated with changes in anthocyanin accumulation (Fig. 6). Anthocyanin biosynthesis appears to be transcriptionally controlled in a cell-autonomous way in response to a light environment of each cell. On the other hand, post-transcriptional regulation might be more important for the metabolic control of photosynthetic pigments (chlorophyll and carotenoid) and products (starch/sugar). It is probably because sugar is transported to sink cells, thus it should be controlled in relation to the other cells, which may necessitate more complex regulatory mechanisms.

Comprehensive transcriptome analyses associated with autumn leaf senescence have been conducted in several plant species (Bhalerao *et al.*, 2003; Wen *et al.*, 2015; Li *et al.*, 2020). Compared to this study, the trend of gradually decreasing expression of photosynthesis-related genes is similar, but the expression of other genes varies according to the phenology of each plant. In aspen (*Populus tremula*), an increase in the expression of metallothionein genes was prominent during autumn leaf senescence (Bhalerao *et al.*, 2003), but it was not observed in maple and other species. Conversely, increased expression of protease-coding genes was observed in both maple and aspen during autumn senescence (Fig. 10), indicating activation of protein degradation is common in these species. In gum trees in a subtropical region (Wen *et al.*, 2015), the expression of genes related to chlorophyll biosynthesis contrasts with that in maple: in gums, key genes such as HEMA and ChlH show decreased expression during summer and increased expression during winter, which probably reflects the phenology of gums maintaining chlorophyll even in winter. The gene expression pattern of *Ginkgo biloba* leaves during autumn

senescence (Li et al., 2020) is relatively similar to that in maple, showing a gradual decrease in the expression of chlorophyll biosynthesis genes and constant expression of carotenoid synthesis genes. It seems that the gene expression patterns associated with autumn senescence exhibit convergent evolution rather than phylogenetic relationships.

The decrease in Chl_{a+b} synchronized with that in leaf N. In IL and LL leaves, increases in $Chl_{a:b}$ were observed on 26 Oct, which might reflect a conversion of chlorophyll b to chlorophyll a for the degradation of light-harvesting complexes (LHC) during leaf senescence (Tanaka & Tanaka, 2011). Key enzymes of chlorophyll biosynthesis, such as HEMA1, CHLH and MGCy-CHL27, were expressed greater in IL leaves than in LL leaves until the onset of leaf senescence (13 Oct) (Fig. 7). In general, the turnover of chlorophyll *a* and *b* in leaves is low (Beisel *et al.*, 2010), where only part of chlorophyll *a* could be degraded in a light-dependent manner, which is probably not catalyzed by enzymes. Thus, the function of de-novo chlorophyll biosynthesis might compensate chlorophyll that was degraded by light-induced damages under high light condition (IL) compared with low light condition (LL). Conversely, enzymes related to chlorophyll breakdown (NYC1, SGR, PPH, and PAO) showed marked increases on 13 Oct at the onset of leaf senescence, which might lead to rapidly declined chlorophyll contents in late Oct. Interestingly, the expressions of these enzymes were highly synchronized during developmental progress and between IL and LL conditions, indicating that chlorophyll degradation is under strict developmental control at whole-tree level, irrespective of the difference in light environments among individual leaves. The decrease in Chl_{a+b} during leaf senescence might be involved in both a decline in chlorophyll biosynthesis and an enhancement of chlorophyll degradation (Tanaka & Tanaka, 2011).

At the onset of leaf senescence (13 Oct), transcriptomic regulation of xanthophyll-related enzymes, ZEP, and VDE was functional. Thus, it would be reasonable to assume that the observed changes in the (V+A)/(V+A+Z) ratios (Fig. 2F) resulted from the changes in the activity of ZEP/VDE. In particular, VDE activity depends on the ΔpH of thylakoid membranes (Pfündel & Dilley, 1993), which are supposed to increase under illumination at relatively low temperatures. Pool size of xanthophyll pigments (V+A+Z) kept relatively higher values in HL leaves than IL and LL leaves from 19 to 26 Oct, suggesting that xanthophyll-related non-photochemical quenching (Demmig-Adams & Adams, 2006) might still be functional in HL leaves at the final stage of leaf senescence. As xanthophyll conversion state (Z+A)/(V+A+Z) is dependent on the light intensity at leaf sampling (Verhoeven *et al.*, 1999; Gamon *et al.*, 2015), higher (Z+A)/(V+A+Z) was

observed in leaves grown under higher light intensities (HL > IL > LL) throughout the season. Increases in (Z+A)/(V+A+Z) observed in IL and LL leaves on 26 Oct might suggest increased thermal energy dissipation that compensated the decrease in energy dissipation by electron flow during leaf senescence (Demmig-Adams *et al.*, 1996; Lu *et al.*, 2002; Kitao *et al.*, 2018, 2019).

Conversely, photoinhibition, indicated by decreased F_v/F_m (Kitao *et al.*, 2022), was not apparent until 26 Oct. However, the values of F_v/F_m (> 0.4) on 26 Oct were considerably higher than that reported in shade-grown seedlings of fullmoon maple (F_v/F_m = 0.25) to repress N resorption, when exposed to full sunlight during leaf senescence (Kitao *et al.*, 2022). Considering that leaf N resorption was also almost completed on 26 Oct, we postulate that photooxidative stress was well managed not to interfere leaf N resorption in all leaves irrespective of growth light conditions.

Based on the multiple regression analysis regarding photoinhibition, greater amount of solar radiation might exacerbate photoinhibition (Werner *et al.*, 2001). Conversely, higher photosynthetic activity indicated by A_{mass} and A_{area} might contribute to preventing photoinhibition in leaves grown under higher solar radiation (Table 1). The role of anthocyanins as a sunscreen or antioxidants (Neill *et al.*, 2002; Hoch *et al.*, 2003; Renner & Zohner, 2019; Moustaka *et al.*, 2020) was not confirmed because of the negative coefficient for leaf anthocyanin contents predicting F_v/F_m (Table 1). Little contribution of anthocyanins as a sunscreen was further supported by the higher leaf absorptance in HL and IL leaves with greater amounts of anthocyanins than in LL leaves during leaf senescence (Fig. 1F). Similarly, accumulation of anthocyanins in Norway maple (*Acer platanoides*) and a purple-colored variety of it might not contribute to alleviating chronic photoinhibition (Rantala *et al.*, 2023; Mattila & Tyystjärvi, 2023). Although a major part of electron flow was consumed by photosynthesis, total electron flow, consumed by Rubisco carboxylation (photosynthesis) and oxygenation (photorespiration), and alternative electron pathways, is more relevant than photosynthetic rate *per se* in terms of preventing PSII from excessive energy accumulation (Foyer *et al.*, 1990; Laisk *et al.*, 2006; Rochaix, 2011). We assumed that ETR calculated by chlorophyll fluorescence empirically represented total electron flow. Maintaining higher ETR in leaves exposed to higher solar radiation (HL leaves) during leaf senescence (18 to 25 Oct) might have a photoprotective role against photoinhibition, together with thermal energy dissipation related to the higher pool size of xanthophyll, as described above (Demmig-Adams *et al.*, 1996; Kitao *et al.*, 2006, 2018).

Regarding the role of anthocyanins as an alternative electron sink, we also made an estimation of alternative electron flow (J_A) consumed by processes other than photosynthesis and photorespiration, based on total electron flow calculated via chlorophyll fluorescence (J_F, equal to ETR), and electron flow consumed by Rubisco carboxylation and oxygenation (J_R); $J_A = J_F - J_R$ (Laisk *et al.*, 2006). Although there might be an inevitable uncertainty in estimating J_R accurately because of many assumptions on the parameters not directly measured, such as C_i-based Γ^* and R_d. However, we believe that assessments of seasonal trends in electron flows and for a relative comparison among leaves grown under different light conditions would be possible. Details about the methods are described in Supplementary data (Methods S3). Alternative electron pathways consist of cyclic electron flow around PSI, water-water cycle, nitrite reduction, and malate valve, adjusting ATP/NADPH ratio during photosynthesis, and also preventing overreduction in the electron transport chain (Foyer *et al.*, 1990; Heber & Walker, 1992; Laisk *et al.*, 2006; Walker *et al.*, 2020). We found that J_A in HL, and IL leaves was higher than that in LL leaves throughout the season (Fig. S10, Table S7). Conversely, the ratio of J_A to J_F in HL and IL leaves was relatively stable throughout the growing season (except for 26 Jul in HL, and 25 Oct in HL and IL leaves), even when J_F declined but substantially high amount of anthocyanins accumulation was observed on 19 Oct in HL and IL leaves (Fig. S11, Table S7). This suggests that the synthesis of anthocyanins might not enhance the amount of J_A relative to J_F. Instead, it might compensate decreases in energy (ATP) and reducing power (NADPH) consumption by other metabolic processes, such as starch synthesis, and protein synthesis during leaf senescence (Keskitalo *et al.*, 2005); the latter is supported by the lack of high-quality RNA on 19 Oct in the present study. Since both anthocyanin and starch biosynthesis was enhanced due to excess of ATP and NADPH in N-limited grape cell suspensions with decreasing protein synthesis (Soubeyrand *et al.*, 2018), anthocyanin biosynthesis may play a relevant role as an alternative electron sink after the cessation of starch synthesis.

Among seasonally-programmed processes, the identical seasonal change in Sugar/(Sugar+Starch) across growth light conditions is a novel finding. The expression of the key genes for starch biosynthesis (AGPase L2 and S) show a gradual decrease, whereas, the expression of the key genes for starch degradation (BAM3 and BAM9), and sucrose synthesis (SPS1) show a gradual increase from 3 Sep to 13 Oct irrespective of growth light conditions. Sugar/(Sugar+Starch) was higher than 0.90 on 19 Oct and higher than 0.96 from 22 to 29 Oct in all leaves, suggesting that starch synthesis might stop completely during the late stage of leaf N

608 resorption. Such a synchronized change in Sugar/(Sugar+Starch) was also observed in the same
609 tree in the previous year, 2020 (across years), and pot-grown seedlings of fullmoon maple under
610 open (full-sunlight) and shade (relative irradiance of ≈ 13% to open) conditions in 2021 (among
611 individuals between different light conditions) (Fig. 11, cf. Kitao et al. 2022). Suppression of
612 starch biosynthesis and enhancement of starch degradation during leaf senescence might be
613 under an accurate temporal regulation for sugar (energy) supply toward the onset of leaf N
614 resorption (Keskitalo *et al.*, 2005; Kim, 2019).

615 As starch is water-insoluble, it acts as an efficient sugar-buffer, accumulating
616 photosynthates in an osmotically inert form (Egger *et al.*, 1996; Kitao *et al.*, 2004; Wyka *et al.*,
617 2016). As the buffer function of starch declined toward leaf senescence, anthocyanins in leaves
618 of fullmoon maple might act as an alternative sugar-buffer, retarding leaf senescence (Fig. 5B**,**
619 Fig. S8) (Ono *et al.*, 2001; Landi *et al.*, 2015; Lo Piccolo *et al.*, 2018; Lo Piccolo & Landi, 2021;
620 Davies *et al.*, 2022), as well as an alternative sink for light energy consumption, maintaining ETR
621 to prevent photoinhibition (Fig. 4B,D) (Hernández & Van Breusegem, 2010; Kitao *et al.*, 2018).
622 Assuming that cyanidin 3-*O*-glucoside was the main anthocyanin in autumn leaves of *A.*
623 *japonicum* (Iwashina & Murai, 2008), the highest anthocyanin (25 μmol g^{-1}) in HL and IL leaves
624 was equivalent to 15.75 mg g^{-1} glucose based on the 3.5 fold difference in the C skeleton.
625 Furthermore, if ATP and reducing power (needed for anthocyanin biosynthesis) are provided
626 from sugars through glycolysis, TCA cycle, and mitochondrial electron transport (Fernie *et al.*,
627 2004), much more glucose should be taken into account. In such a case, anthocyanins could be
628 considered as an effective energy escape valve, maintaining photosynthetic electron flow to
629 prevent photoinhibition even under starch depletion (Mattila & Tyystjärvi, 2023).

630 A marked increase in F3GlcT observed in IL leaves on 13 Oct that corresponded to an
631 increase in Sugar/(Sugar+Starch) also supports this hypothesis. The fewer amounts of
632 anthocyanins in LL leaves might be attributed to the lower production of photosynthates under
633 the low light condition. This appears to be consistent with anthocyanins being mainly found in
634 central vacuoles, apart from cytoplasmatic and chloroplastic metabolism (Merzlyak *et al.*, 2008),
635 which is often referred as a rebuttal against the role of anthocyanins as antioxidants in
636 “photoprotection hypothesis” (Archetti *et al.*, 2009; Hughes *et al.*, 2022). Merzlyak et al. (2008)
637 also reported that anthocyanins accumulated in the vacuoles of the epidermis in spring, but in
638 the vacuoles of the palisade parenchyma in autumn. The former might be a photoprotective
639 strategy (sunscreen) for immature photosynthetic machinery in young leaves, as proposed in

"photoprotection hypothesis" (Archetti *et al.*, 2009; Renner & Zohner, 2019, 2020), but the latter might support the idea that anthocyanins act as a sugar-buffer and an alternative sink for electron transport.

Thus, as "holocanopy hypothesis" posits, anthocyanins protected outer-canopy leaves against early-shedding and photoinhibition, then the outer-canopy leaves protected inner-canopy leaves from photoinhibition by shading (cf. Kitao et al. 2022), which contributes to efficient N resorption as a whole tree. As for protecting outer-canopy leaves against strong light, "holocanopy hypothesis" might be on the side of "photoprotective hypothesis" rather than "co-evolution hypothesis". However, underlying mechanisms involved in anthocyanins were substantially different; a sugar-buffer and an alternative electron sink for the former, *versus* sunscreen and antioxidants for the latter (Archetti *et al.*, 2009). Furthermore, "holocanopy hypothesis" might comprehend "nutrient-limitation hypothesis", which recently proposes that low leaf N and high soluble sugars may serve as the proximate causes for autumn leaf reddening (Hughes *et al.*, 2022).

Regarding non-anthocyanic species, silver birch (*Betula pendula*), which usually does not synthesize large amounts of anthocyanins, increases flavonol content with chlorophyll degradation during autumn senescence (Mattila *et al.*, 2018, 2021). Greater accumulation of flavonol glycosides was observed in autumn than in spring in Cabernet Sauvignon grapevine, a cultivar of *Vitis vinifera* L. (Bouderias *et al.*, 2020). Although further investigation is needed, accumulation of flavonoids (including anthocyanins and flavonols) might be a common mechanism to compensate the closed pathway of starch synthesis during leaf senescence, whereas accumulation of anthocyanins or flavonols might be species-specific, leading to a different color appearance (red or yellow) in autumn.

Supplementary data

The following Supplementary data is available for this article:

Suppl. Data Table 1 The list of *Acer japonicum* genes (transcriptome units) that were selected first selected by CDS-HIT, and by BLAST search against the TAIR 10 database.

Suppl. Data Table 2 The list of genes categorized in Clusters A to D by k-Mean clustering.

669 **Suppl. Data Table 3** List of *Acer japonicum* genes that are involved in the metabolism of
670 flavonoid, chlorophyll, carotenoid, starch and sugar.

671 **Methods S1** *Isoform sequencing analysis.*

672 **Methods S2** *Estimation of full-length protein sequences using the Iso-Seq data.*

673 **Methods S3** *Estimation of alternative electron flow*.

674 **Figure S1** Phenological records of *Acer japonicum*.

675 **Figure S2** Seasonal changes in daily integrated photosynthetic active radiance, and in daily mean
676 temperature.

677 **Figure S3** Principle component analysis (PCA) of *Acer japonicum* transcriptomes.

678 **Figure S4** k-means clustering shows four clusters of *Acer japonicum* transcriptomes.

679 **Figure S5** Seasonal changes in leaf mass per area (LMA) in leaves grown under different light
680 conditions within the canopy of fullmoon maple tree.

681 **Figure S6** Seasonal changes in mean PAR for 1 h before leaf sampling for leaves grown under
682 different light conditions within the canopy of fullmoon maple.

683 **Figure S7** Relationship between leaf anthocyanin and sugar contents in leaves grown at the
684 south-faced outer-canopy, north-faced outer-canopy, and north-faced inner-canopy of an adult
685 tree of fullmoon maple.

686 **Figure S8** Relationships between [Sugar/(Sugar+Starch)] and $Anthocyanin_{mass}$, and between
687 $Anthocyanin_{mass}$ and $Sugar_{mass}$.

688 **Figure S9** Seasonal changes in 2020.

689 **Figure S10** Seasonal changes in J_F, J_R, and J_A.

690 **Figure S11** Seasonal changes in the ratio of J_A to J_F.

691 **Table S1** Representative metabolic pathways enriched in k-means clustering. Top 1,000 genes.

692 **Table S2** Results of Tukey-Kramer multiple comparison test of dry mass- and area-based leaf
693 anthocyanin content, leaf N content, and F_v/F_m in leaves of a fullmoon maple tree among dates,
694 or among light conditions.

Table S3 Results of Tukey-Kramer multiple comparison test of leaf mass per area (LMA) in leaves of a fullmoon maple tree among dates, or among light conditions.

Table S4 Results of Tukey-Kramer multiple comparison test of pigments in leaves of a fullmoon maple tree among date, or among light conditions.

Table S5 Results of Tukey-Kramer multiple comparison test of dry mass- and area-based leaf sugar content, leaf starch content, and ratio of sugar to [sugar + starch] in leaves of a fullmoon maple tree among date, or among light conditions.

Table S6 Results of Tukey-Kramer multiple comparison test of dry mass- and area-based net photosynthetic rate, and electron transport rate in leaves of a fullmoon maple tree among dates, or among light conditions.

Table S7 Results of Tukey-Kramer multiple comparison test of J_F, J_R, J_A, and J_A/J_F in leaves of a fullmoon maple tree among dates, or among light conditions.

Acknowledgements

We thank H. Yamamoto for her skillful technical assistance.

Competing interests

None declared.

Author contributions

Mitsutoshi Kitao: Conceptualization, Investigation, Formal analysis, Writing - Original Draft. Kenichi Yazaki: Investigation, Writing - Review & Editing. Hiroyuki Tobita: Investigation, Writing - Review & Editing. Evgenios Agathokleous: Validation, Writing - Review & Editing. Junko Kishimoto: Investigation, Writing - Review & Editing. Atsushi Takabayashi: Investigation, Writing - Review & Editing. Ryouichi Tanaka: Conceptualization, Investigation, Writing - Review & Editing.

Funding

This study was supported in part by JSPS KAKENHI, Grant Numbers JP20H03036, JP20H03017, JP23H02262, and JP23H04960.

Data availability

The datasets generated by this study are deposited at the NCBI Gene Expression Omnibus public database under the accession numbers PSUB020351, PRJDB15855, and PRJDB15856.

References

Altschul SF, Gish W, Miller W, Myers EW, Lipman DJ. **1990**. Basic local alignment search tool. *Journal of Molecular Biology* **215**: 403–410.

Anjum NA, Sofo A, Scopa A, Roychoudhury A, Gill SS, Iqbal M, Lukatkin AS, Pereira E, Duarte AC, Ahmad I. **2015**. Lipids and proteins—major targets of oxidative modifications in abiotic stressed plants. *Environmental Science and Pollution Research* **22**: 4099–4121.

Aramaki T, Blanc-Mathieu R, Endo H, Ohkubo K, Kanehisa M, Goto S, Ogata H. **2020**. KofamKOALA: KEGG Ortholog assignment based on profile HMM and adaptive score threshold. *Bioinformatics* **36**: 2251–2252.

Archetti M, Döring TF, Hagen SB, Hughes NM, Leather SR, Lee DW, Lev-Yadun S, Manetas Y, Ougham HJ, Schaberg PG, *et al.* 2009. Unravelling the evolution of autumn colours: an interdisciplinary approach. *Trends in Ecology and Evolution* **24**: 166–173.

Beisel KG, Jahnke S, Hofmann D, Köppchen S, Schurr U, Matsubara S. **2010**. Continuous Turnover of Carotenes and Chlorophyll a in Mature Leaves of Arabidopsis Revealed by $^{14}CO_2$ Pulse-Chase Labeling. *Plant Physiology* **152**: 2188–2199.

Bhalerao R, Keskitalo J, Sterky F, Erlandsson R, Björkbacka H, Birve SJ, Karlsson J, Gardeström P, Gustafsson P, Lundeberg J, *et al.* 2003. Gene expression in autumn leaves. *Plant Physiology* **131**: 430–442.

Bouderias S, Teszlák P, Jakab G, Kőrösi L. **2020**. Age- and season-dependent pattern of flavonol glycosides in Cabernet Sauvignon grapevine leaves. *Scientific Reports* **10**: 14241.

Chen S, Zhou Y, Chen Y, Gu J. **2018**. fastp: an ultra-fast all-in-one FASTQ preprocessor. *Bioinformatics* **34**: i884–i890.

Cornic G, Fresneau C. **2002**. Photosynthetic carbon reduction and carbon oxidation cycles are the main electron sinks for photosystem II activity during a mild drought. *Annals of Botany* **89**: 887–894.

Davies KM, Landi M, van Klink JW, Schwinn KE, Brummell DA, Albert NW, Chagné D, Jibran R, Kulshrestha S, Zhou Y, *et al.* 2022. Evolution and function of red pigmentation in land plants. *Annals of Botany* **130**: 613–636.

Demmig-Adams B, Adams WW. **2006**. Photoprotection in an ecological context: The remarkable complexity of thermal energy dissipation. *New Phytologist* **172**: 11–21.

Demmig-Adams B, Adams III WW, Barker DH, Logan BA, Bowling DR, Verhoeven AS. **1996**. Using chlorophyll fluorescence to assess the fraction of absorbed light allocated to thermal dissipation of excess excitation. *Physiologia Plantarum* **98**: 253–264.

Egger B, Einig W, Schlereth A, Wallenda T, Magel E, Loewe A, Hampp RRR, Sclereth A, Wallenda T, Magel E, *et al.* 1996. Carbohydrate metabolism in one- and two-year-old spruce needles, and stem carbohydrates from three months before until three months after bud break. *Physiologia Plantarum* **96**: 91–100.

Feild TS, Lee DW, Holbrook NM. **2001**. Why leaves turn red in autumn. The role of anthocyanins in senescing leaves of red-osier dogwood. *Plant Physiology* **127**: 566–574.

Fernie AR, Carrari F, Sweetlove LJ. **2004**. Respiratory metabolism: glycolysis, the TCA cycle and mitochondrial electron transport. *Current Opinion in Plant Biology* **7**: 254–261.

Foyer C, Furbank R, Harbinson J, Horton P. **1990**. The mechanisms contributing to photosynthetic control of electron transport by carbon assimilation in leaves. *Photosynthesis Research* **25**: 83–100.

Fracheboud Y, Luquez V, Björkén L, Sjödin A, Tuominen H, Jansson S. **2009**. The control of autumn senescence in European aspen. *Plant Physiology* **149**: 1982–1991.

Gamon JA, Kovalchuck O, Wong CYS, Harris A, Garrity SR. **2015**. Monitoring seasonal and diurnal changes in photosynthetic pigments with automated PRI and NDVI sensors. *Biogeosciences* **12**: 4149–4159.

Ge SX, Son EW, Yao R. **2018**. iDEP: an integrated web application for differential expression and pathway analysis of RNA-Seq data. *BMC Bioinformatics* **19**: 534.

Genty B, Briantais J-MM, Baker NR. **1989**. The relationship between the quantum yield of photosynthetic electron transport and quenching of chlorophyll fluorescence. *Biochimica et Biophysica Acta - General Subjects* **990**: 87–92.

Heber U, Walker D. **1992**. Concerning a dual function of coupled cyclic electron transport in leaves. *Plant Physiology* **100**: 1621–1626.

Hendrickson L, Furbank RT, Chow WS. **2004**. A simple alternative approach to assessing the fate of absorbed light energy using chlorophyll fluorescence. *Photosynthesis Research* **82**: 73–81.

Henriques R, Calderan-Rodrigues MJ, Luis Crespo J, Baena-González E, Caldana C. **2022**. Growing of the TOR world. *Journal of Experimental Botany* **73**: 6987–6992.

Hernández I, Van Breusegem F. **2010**. Opinion on the possible role of flavonoids as energy escape valves: Novel tools for nature's Swiss army knife? *Plant Science* **179**: 297–301.

Hoch WA, Singsaas EL, McCown BH. **2003**. Resorption protection. Anthocyanins facilitate nutrient recovery in autumn by shielding leaves from potentially damaging light levels. *Plant Physiology* **133**: 1296–1305.

Hoch WA, Zeldin EL, McCown BH. **2001**. Physiological significance of anthocyanins during autumnal leaf senescence. *Tree Physiology* **21**: 1–8.

Horton P, Ruban AV, Walters RG. **1996**. Regulation of light harvesting in green plants. *Annual Review of Plant Physiology and Plant Molecular Biology* **47**: 655–684.

Huber SC, Huber JL. **1996**. Role and regulation of sucrose-phosphate synthase in higher plants. *Annual Review of Plant Physiology and Plant Molecular Biology* **47**: 431–444.

Hughes NM, George CO, Gumpman CB, Neufeld HS. **2022**. Coevolution and photoprotection as

complementary hypotheses for autumn leaf reddening: a nutrient-centered perspective. *New Phytologist* **233**: 22–29.

Iwashina T, Murai Y. **2008**. Quantitative variation of anthocyanins and other flavonoids in autumn leaves of *Acer palmatum*. *Bulletin of the National Museum of Nature and Science Series B (Botany)* **34**: 53–62.

Keskitalo J, Bergquist G, Gardeström P, Jansson S. **2005**. A cellular timetable of autumn senescence. *Plant Physiology* **139**: 1635–1648.

Kikuzawa K. **1983**. Leaf survival of woody plants in deciduous broad-leaved forests. 1. Tall trees. *Canadian Journal of Botany* **61**: 2133–2139.

Kim J. **2019**. Sugar metabolism as input signals and fuel for leaf senescence. *Genes & Genomics* **41**: 737–746.

Kitao M, Kitaoka S, Harayama H, Tobita H, Agathokleous E, Utsugi H. **2018**. Canopy nitrogen distribution is optimized to prevent photoinhibition throughout the canopy during sun flecks. *Scientific Reports* **8**: 503.

Kitao M, Lei TTT, Koike T, Tobita H, Maruyama Y. **2006**. Tradeoff between shade adaptation and mitigation of photoinhibition in leaves of *Quercus mongolica* and *Acer mono* acclimated to deep shade. *Tree Physiology* **26**: 441–448.

Kitao M, Qu L, Koike T, Tobita H, Maruyama Y. **2004**. Increased susceptibility to photoinhibition in pre-existing needles experiencing low temperature at spring budbreak in Sakhalin spruce (*Picea glehnii*) seedlings. *Physiologia Plantarum* **122**: 226–232.

Kitao M, Tobita H, Kitaoka S, Harayama H, Yazaki K, Komatsu M, Agathokleous E, Koike T. **2019**. Light energy partitioning under various environmental stresses combined with elevated CO_2 in three deciduous broadleaf tree species in Japan. *Climate* **7**: 79.

Kitao M, Yazaki K, Tobita H, Agathokleous E, Kishimoto J, Takabayashi A, Tanaka R. **2022**. Exposure to strong irradiance exacerbates photoinhibition and suppresses N resorption during leaf senescence in shade-grown seedlings of fullmoon maple (*Acer japonicum*). *Frontiers in Plant Science* **13**: 1006413.

Klughammer C, Schreiber U. **2008**. Complementary PS II quantum yields calculated from simple fluorescence parameters measured by PAM fluorometry and the Saturation Pulse method. *PAM Application Notes* **1**: 27–35.

Koike T. **1990**. Autumn coloring, photosynthetic performance and leaf development of deciduous broad-leaved trees in relation to forest succession. *Tree Physiology* **7**: 21–32.

Koike T. **2004**. Autumn Coloration, Carbon Acquisition and Leaf Senescence. In: Plant Cell Death Processes. Academic Press, 245–258.

Laisk A, Eichelmann H, Oja V, Rasulov B, Rämma H. **2006**. Photosystem II cycle and alternative electron flow in leaves. *Plant and Cell Physiology* **47**: 972–983.

Landi M, Tattini M, Gould KS. **2015**. Multiple functional roles of anthocyanins in plant-environment interactions. *Environmental and Experimental Botany* **119**: 4–17.

Li W, Wang L, He Z, Lu Z, Cui J, Xu N, Jin B, Wang L. **2020**. Physiological and transcriptomic changes during autumn coloration and senescence in *Ginkgo biloba* leaves. *Horticultural Plant Journal* **6**: 396–408.

Lim E-K, Li Y, Parr A, Jackson R, Ashford DA, Bowles DJ. **2001**. Identification of glucosyltransferase genes involved in sinapate metabolism and lignin synthesis in *Arabidopsis*. *Journal of Biological Chemistry* **276**: 4344–4349.

Lo Piccolo E, Landi M. **2021**. Red-leafed species for urban "greening" in the age of global climate change. *Journal of Forestry Research* **32**: 151–159.

Lo Piccolo E, Landi M, Pellegrini E, Agati G, Giordano C, Giordani T, Lorenzini G, Malorgio F, Massai R, Nali C, *et al.* 2018. Multiple consequences induced by epidermally-located anthocyanins in young, mature and senescent leaves of *Prunus*. *Frontiers in Plant Science* **9**: 917.

Lohman KN, Gan S, John MC, Amasino RM. **1994**. Molecular analysis of natural leaf senescence in *Arabidopsis thaliana*. *Physiologia Plantarum* **92**: 322–328.

Long SP, Humphries S, Falkowski PG. **1994**. Photoinhibition of photosynthesis in nature. *Annual Review of Plant Physiology and Plant Molecular Biology* **45**: 633–662.

Lu Q, Lu C, Zhang J, Kuang T. **2002**. Photosynthesis and chlorophyll a fluorescence during flag leaf senescence of field-grown wheat plants. *Journal of Plant Physiology* **159**: 1173–1178.

Lu Y, Sharkey TD. **2006**. The importance of maltose in transitory starch breakdown. *Plant, Cell & Environment* **29**: 353–366.

Lunn JE, Delorge I, Figueroa CM, Van Dijck P, Stitt M. **2014**. Trehalose metabolism in plants. *The Plant Journal* **79**: 544–567.

Mattila H, Sotoudehnia P, Kuuslampi T, Stracke R, Mishra KB, Tyystjärvi E. **2021**. Singlet oxygen, flavonols and photoinhibition in green and senescing silver birch leaves. *Trees* **35**: 1267–1282.

Mattila H, Tyystjärvi E. **2023**. Red pigments in autumn leaves of Norway maple do not offer significant photoprotection but coincide with stress symptoms. *Tree Physiology* **43**: 751–768.

Mattila H, Valev D, Havurinne V, Khorobrykh S, Virtanen O, Antinluoma M, Mishra KB, Tyystjärvi E. **2018**. Degradation of chlorophyll and synthesis of flavonols during autumn senescence-the story told by individual leaves. *AoB PLANTS* **10**.

Merzlyak MN, Chivkunova OB, Solovchenko AE, Naqvi KR. **2008**. Light absorption by anthocyanins in juvenile, stressed, and senescing leaves. *Journal of Experimental Botany* **59**: 3903–3911.

Moustaka J, Tanou G, Giannakoula A, Adamakis I-DS, Panteris E, Eleftheriou EP, Moustakas M. **2020**. Anthocyanin accumulation in poinsettia leaves and its functional role in photo-oxidative stress. *Environmental and Experimental Botany* **175**: 104065.

Murchie EH, Ruban AV. **2020**. Dynamic non-photochemical quenching in plants: from molecular mechanism to productivity. *The Plant Journal* **101**: 885–896.

Neill SO, Gould KS, Kilmartin PA, Mitchell KA, Markham KR. **2002**. Antioxidant activities of red versus green leaves in *Elatostema rugosum*. *Plant, Cell & Environment* **25**: 539–547.

Ono K, Nishi Y, Watanabe A, Terashima I. **2001**. Possible mechanisms of adaptive leaf senescence. *Plant Biology* **3**: 234–243.

de Pascual-Teresa S, Sanchez-Ballesta MT. **2008**. Anthocyanins: from plant to health. *Phytochemistry Reviews* **7**: 281–299.

Patro R, Duggal G, Love MI, Irizarry RA, Kingsford C. **2017**. Salmon provides fast and bias-aware quantification of transcript expression. *Nature Methods* **14**: 417–419.

Pena-Novas I, Archetti M. **2020**. Biogeography and evidence for adaptive explanations of autumn colors. *New Phytologist* **228**: 809–813.

Pena-Novas I, Archetti M. **2021**. A test of the photoprotection hypothesis for the evolution of autumn colours: Chlorophyll resorption, not anthocyanin production, is correlated with nitrogen translocation. *Journal of Evolutionary Biology* **34**: 1423–1431.

Pfündel EE, Dilley RA. **1993**. The pH dependence of violaxanthin deepoxidation in isolated pea chloroplasts. *Plant Physiology* **101**: 65–71.

R Core Team, R Development Core Team. **2020**. *R: A Language and Environment for Statistical Computing*.

Rantala M, Mulo P, Tyystjärvi E, Mattila H. **2023**. Biophysical and molecular characteristics of senescing leaves of two Norway maple varieties differing in anthocyanin content. *Physiologia Plantarum* **175**: e13999.

Renner SS, Zohner CM. **2019**. The occurrence of red and yellow autumn leaves explained by regional differences in insolation and temperature. *New Phytologist* **224**: 1464–1471.

Renner SS, Zohner CM. **2020**. Further analysis of 1532 deciduous woody species from North America, Europe, and Asia supports continental-scale differences in red autumn colouration. *New Phytologist* **228**: 814–815.

Rochaix J-D. **2011**. Regulation of photosynthetic electron transport. *Biochimica et Biophysica Acta (BBA) - Bioenergetics* **1807**: 375–383.

Ruban AV. **2016**. Nonphotochemical chlorophyll fluorescence quenching: Mechanism and effectiveness in protecting plants from photodamage. *Plant Physiology* **170**: 1903–1916.

Saito K, Yonekura-Sakakibara K, Nakabayashi R, Higashi Y, Yamazaki M, Tohge T, Fernie AR. **2013**. The flavonoid biosynthetic pathway in Arabidopsis: Structural and genetic diversity. *Plant Physiology and Biochemistry* **72**: 21–34.

Shameer S, Ratcliffe RG, Sweetlove LJ. **2019**. Leaf energy balance requires mitochondrial

respiration and export of chloroplast NADPH in the light. *Plant Physiology* **180**: 1947–1961.

Soubeyrand E, Colombié S, Beauvoit B, Dai Z, Cluzet S, Hilbert G, Renaud C, Maneta-Peyret L, Dieuaide-Noubhani M, Mérillon J-M, *et al.* 2018. Constraint-based modeling highlights cell energy, redox status and α-ketoglutarate availability as metabolic drivers for anthocyanin accumulation in grape cells under nitrogen limitation. *Frontiers in Plant Science* **9**.

Stitt M, Hurry V. **2002**. A plant for all seasons: alterations in photosynthetic carbon metabolism during cold acclimation in *Arabidopsis*. *Current Opinion in Plant Biology* **5**: 199–206.

Streb S, Zeeman SC. **2012**. Starch metabolism in *Arabidopsis*. *The Arabidopsis Book* **2012**.

Tanaka R, Tanaka A. **2011**. Chlorophyll cycle regulates the construction and destruction of the light-harvesting complexes. *Biochimica et Biophysica Acta (BBA) - Bioenergetics* **1807**: 968–976.

Tohge T, Nishiyama Y, Hirai MY, Yano M, Nakajima J, Awazuhara M, Inoue E, Takahashi H, Goodenowe DB, Kitayama M, *et al.* 2005. Functional genomics by integrated analysis of metabolome and transcriptome of Arabidopsis plants over-expressing an MYB transcription factor. *The Plant Journal* **42**: 218–235.

Verhoeven AS, Adams WW, Demmig-Adams B. **1999**. The xanthophyll cycle and acclimation of *Pinus ponderosa* and *Malva neglecta* to winter stress. *Oecologia* **118**: 277–287.

Walker BJ, Kramer DM, Fisher N, Fu X. **2020**. Flexibility in the energy balancing network of photosynthesis enables safe operation under changing environmental conditions. *Plants* **9**: 301.

Wallace TC, Giusti MM. **2015**. Anthocyanins. *Advances in Nutrition* **6**: 620–622.

Wen C-H, Lin S-S, Chu F-H. **2015**. Transcriptome analysis of a subtropical deciduous tree: Autumn leaf senescence gene expression profile of Formosan gum. *Plant and Cell Physiology* **56**: 163–174.

Werner C, Ryel RJ, Correia O, Beyschlag W. **2001**. Effects of photoinhibition on whole-plant carbon gain assessed with a photosynthesis model. *Plant, Cell & Environment* **24**: 27–40.

Wingler A, Delatte TL, O'Hara LE, Primavesi LF, Jhurreea D, Paul MJ, Schluepmann H. **2012**. Trehalose 6-phosphate is required for the onset of leaf senescence associated with high carbon availability. *Plant Physiology* **158**: 1241–1251.

Wingler A, Purdy S, MacLean JA, Pourtau N. **2006**. The role of sugars in integrating environmental signals during the regulation of leaf senescence. *Journal of Experimental Botany* **57**: 391–399.

Wurzinger B, Nukarinen E, Nägele T, Weckwerth W, Teige M. **2018**. The SnRK1 kinase as central mediator of energy signaling between different organelles. *Plant Physiology* **176**: 1085–1094.

Wyka TP, Żytkowiak R, Oleksyn J. **2016**. Seasonal dynamics of nitrogen level and gas exchange in different cohorts of Scots pine needles: a conflict between nitrogen mobilization and photosynthesis? *European Journal of Forest Research* **135**: 483–493.

Table 1. Summary of multiple linear regression of F_v/F_m in leaves grown under different light conditions in the canopy of fullmoon maple. Initial explanatory variables affecting F_v/F_m: daily mean temperature, and dry mass- or area-based integrated solar radiation ($PAR_{int.mass}$, $PAR_{int,area}$), light-saturated net photosynthetic rate (A_{mass}, A_{area}) in the previous day of F_v/F_m measurements, xanthophyll pigments content ($V+A+Z_{mass,}$ $V+A+Z_{area}$), including violaxanthin (V), antheraxanthin (A), and zeaxanthin (Z), anthocyanins content, which were determined in leaves just after F_v/F_m measurements. Area-based integrated solar radiation ($PAR_{int,area}$) was converted to mass-based $PAR_{int.mass}$ as $[PAR_{int,area}]$/LMA (= leaf mass per area). Stepwise regressions were undertaken to define the subset of effects that would altogether provide the smallest corrected Akaike information criterion (AIC) in subsequent modeling. As a measure of multicollinearity, variance inflation factor (VIF) is demonstrated.

	Summary measures		Regression coefficients					
	R^2	*P*	Intercept	Variable	Coefficients	t-value	*P*	VIF
Mass-based full model AIC = −263	0.725 (n=96)	< 0.001	0.653	Temperature	−0.00103	−0.69	0.49	1.85
				$PAR_{.int.mass}$	−0.124	−1.88	0.06	2.18
				A_{mass}	2.01	7.48	< 0.001	2.81
				$V+A+Z_{mass}$	−0.0209	−0.43	0.67	3.50
				$Anthocyanin_{mass}$	−0.00734	−4.00	< 0.001	2.48
Mass-based best model AIC = -266	0.729 (n=96)	<0.001	0.637	$PAR_{int.mass}$	−0.152	−3.05	< 0.001	1.30
				A_{mass}	1.93	7.77	< 0.001	2.43
				$Anthocyanin_{mass}$	−0.00672	−3.98	< 0.001	2.12
Area-based full model AIC = −248	0.679 (n=96)	< 0.001	0.650	Temperature	0.000953	0.62	0.54	1.71
				$PAR_{.int.aea}$	−0.00642	−3.71	< 0.001	5.05
				A_{area}	0.0350	7.22	< 0.001	3.01
				$V+A+Z_{area}$	0.000563	0.59	0.56	5.08
				$Anthocyanin_{area}$	−0.123	−3.59	< 0.001	2.28
Area-based best model AIC = −251	0.683 (n=96)	<0.001	0.669	$PAR_{int.area}$	−0.00548	−4.71	< 0.001	2.30
				A_{area}	0.0358	7.57	< 0.001	2.89
				$Anthocyanin_{area}$	−0.139	−4.83	< 0.001	1.64

Figure legends

Figure 1. Seasonal changes in dry mass-based leaf anthocyanin content ($Anthocyanin_{mass}$, A), and leaf N content (N_{mass}, B), area-based leaf anthocyanin content ($Anthocyanin_{area}$, C), and leaf N content (N_{area}, D), F_v/F_m (E), and LED-specific leaf absorptance (ABS_{LED}, F) in leaves grown under high light at the south-faced outer-canopy (red circles, HL), intermediate light at north-faced outer-canopy (open rectangles, IL), and low light at north-faced inner-canopy (black closed triangles, LL) of an adult tree of fullmoon maple. Values are means ± SE (n=4). Insets enlarge seasonal changes in anthocyanins from the end of July to the middle of October. Leaves were sampled after the measurements of F_v/F_m on 27 Jul, 17 Aug, 7 Sep, 28 Sep, 5 Oct, 13 Oct, 19 Oct, 22 Oct, 26 Oct, and 29 Oct. Note: Leaf anthocyanins and N can be measured for the leaves sampled on 29 Oct, whereas F_v/F_m could not be measured, since fluorescence signals were too small because of almost no chlorophyll remained at that time (cf. Fig. 2).

Figure 2. Seasonal changes in dry mass-based leaf chlorophyll content ($Chl_{a+b,mass}$, A), xanthophyll pigment pool size ($V+A+Z_{mass}$, B), area-based leaf chlorophyll content ($Chl_{a+b,area}$, C), xanthophyll pigment pool size ($V+A+Z_{area}$, D), the ratio of chlorophyll a to b ($Chl_{a:b}$, E), and conversion state of xanthophyll cycle [(Z+A)/(V+A+Z), F] in leaves grown at the south-faced outer-canopy (red circles, HL), north-faced outer-canopy (open rectangles, IL), and north-faced inner-canopy (black closed triangles, LL) of an adult tree of fullmoon maple. Values are means ± SE (n=4). Leaves were sampled on 27 Jul, 17 Aug, 7 Sep, 28 Sep, 5 Oct, 13 Oct, 19 Oct, 22 Oct, 26 Oct, and 29 Oct. Note: $Chl_{a:b}$ and (Z+A)/(V+A+Z) could not be calculated on 29 Oct, since the values of Chl_{a+b} and (V+A+Z) were not detectable (=0).

Figure 3. Seasonal changes in mass-based leaf sugar ($Sugar_{mass}$, A) and starch content ($Starch_{mass}$, B), area-based leaf sugar ($Sugar_{area}$, C) and starch content ($Starch_{area}$, D), and the ratio of leaf sugar to [sugar + starch] (Sugar/(Sugar + Starch), E) in leaves grown at the south-faced outer-canopy (red circles, HL), north-faced outer-canopy (open rectangles, IL), and north-faced inner-canopy (black closed triangles, LL) of an adult tree of fullmoon maple. Values are means ± SE (n=4). Leaves were sampled on 27 Jul, 17 Aug, 7 Sep, 28 Sep, 5 Oct, 13 Oct, 19 Oct, 22 Oct, 26 Oct, and 29 Oct.

Figure 4. Seasonal changes in mass-based net photosynthetic rate (A_{mass}, A), electron transport rate (ETR_{mass}, B), area-based net photosynthetic rate (A_{area}, C), and electron transport rate (ETR_{area}, D) in leaves grown at the south-faced outer-canopy (red circles, HL), north-faced outer-canopy (open rectangles, IL), and north-faced inner-canopy (black closed triangles, LL) of an adult tree of fullmoon maple. Measurements were conducted under saturating light (1000 μmol m^{-2} s^{-1}) and optimal leaf temperature ranged from 20 to 25 °C. Values are means ± SE (n=4). Measurements of gas exchange and chlorophyll fluorescence were conducted totally 8 times: 26 Jul, 16 Aug, 6 Sept, 27 Sept, 4 Oct, 12 Oct, 18 Oct, and 25 Oct in 2021.

Figure 5. Relationships between the ratio of sugar to sugar plus starch [Sugar/(Sugar+Starch)] and $Anthocyanin_{mass}$ (A), and between $Anthocyanin_{mass}$ and $Sugar_{mass}$ (B), in leaves grown at the south-faced outer-canopy (red circles, HL), north-faced outer-canopy (open rectangles, IL), and north-faced inner-canopy (black closed triangle, LL) of an adult tree of fullmoon maple.

Figure 6. Expression of genes encoding key enzymes in flavonoid biosynthesis. The x-axes and the y-axes indicate dates and transcripts per million counts (TPM). Open rectangles indicate IL leaves, and black closed triangles LL leaves. Error bars indicate standard deviation (n = 3). Phenylalanine ammonia lyase (PAL) and accetyl-CoA carboxylase (ACC) are key enzymes to control the metabolic flow in anthocyanin synthesis (Saito *et al.*, 2013). Chalcone synthase (CHS) catalyzes the formation of naringenin chalcone, which is the committed step of all flavonoid compounds. This compound is further modified by several enzymes including flavonoid 3' hydroxylase (F3'H) to form cyanidin or related compounds. These compounds are further glycosylated by various glycosylases, including flavonoid 3-O-glucosyltransferase (F3GlcT; also called anthocyanin glycosyltranferase (Tohge *et al.*, 2005), and are stored in the vacuole.

Figure 7. Expression of genes encoding key enzymes in chlorophyll biosynthesis and breakdown. The x-axes and the y-axes indicate dates and transcripts per million counts (TPM). Open rectangles indicate IL leaves, and black closed triangles LL leaves. Error bars indicate standard deviation (n = 3).

Figure 8. Expression of genes encoding key enzymes in carotenoid biosynthesis. The x-axes and the y-axes indicate dates and transcripts per million counts (TPM). Open rectangles indicate IL leaves, and black closed triangles LL leaves. Error bars indicate standard deviation (n = 3).

Figure 9. Expression of the genes encoding the key enzymes in carbohydrate metabolism, related to starch biosynthesis (A) and degradation (B). The X axes and the Y axes indicate dates and transcripts per million counts (TPM). Open rectangles indicate IL leaves, and black closed triangles LL leaves. Error bars indicate standard deviation (n = 3). TP: triose phosphate, G1P: glucose-1-phosphate, F1,6BP: fructose 1,6-bisphosphate. Note: RBCL is encoded by the plastid genome so that it was not expected to be detected after the purification of polyA mRNA for Iso-Seq analysis. Nevertheless, our Iso-Seq analysis detected a small amount of RbcL mRNA, which was possibly due to non-specific binding to the oligo-dT column.

Figure 10. Expression of the genes related to the progression of leaf senescence. HXK denotes hexokinase. TOR is a protein kinase involved in the regulation of various developmental controls. RAPTOR is also involved in developmental controls by interacting with TOR. TPS denotes trehalose phosphate synthase. The numbers following TPS indicates the isoform numbers of the corresponding Arabidopsis homologs. An enzyme that catalyzes the formation of trehalose from trehalose-6-phosphate (T6P) was not detected in our Iso-Seq analysis. SAG12 (senescence-associated gene 12) encodes a vacuolar cysteine protease whose expression is well correlated with the progression of leaf senescence. The X axes and the Y axes indicate dates and transcripts per million counts (TPM). Open rectangles show gene expression under LL conditions, while black closed triangles indicate gene expression under IL conditions. Error bars indicate standard deviation. n = 3.

Figure 11. Seasonal changes in Sugar/(Sugar+Starch) in leaves of an adult tree of fullmoon maple grown under different light conditions in 2021 (cf. Fig. 4E) (A) and in 2020 (n=4 to 6) (cf. Fig. S9J) (B) in leaves grown at the south-faced outer-canopy (red circles, HL), north-faced outer-canopy (open rectangles, IL), and north-faced inner-canopy (black closed triangle, LL) of an adult tree of

fullmoon maple, and that in pot-grown seedlings of fullmoon maple (4-year-old, ≈ 40 cm in shoot height) grown under open (open diamonds) (n=4) and shade: ≈13% of full sunlight (black closed triangles-down) in 2021 (n = 4 to 6) (C) (cf. Kitao et al. 2022). Error bars indicate standard error.

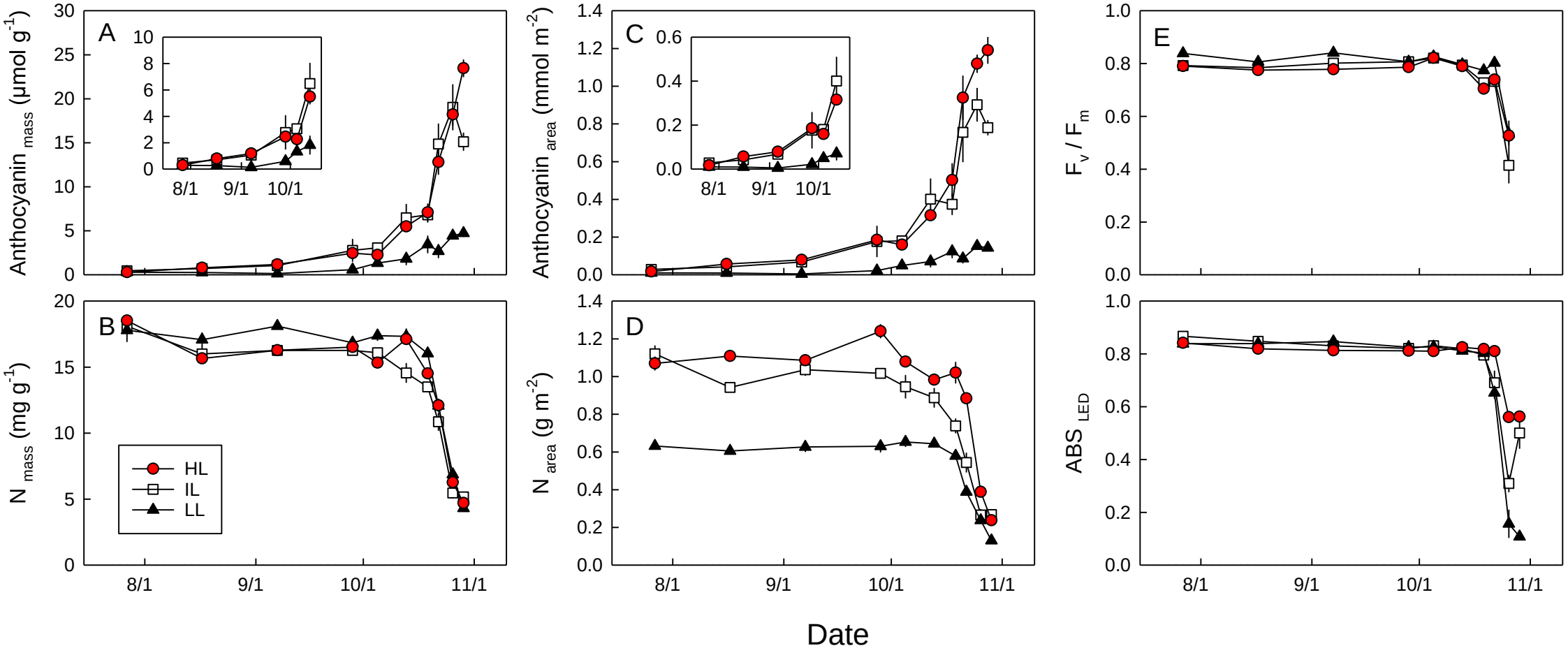

Figure 1. Seasonal changes in dry mass-based leaf anthocyanin content ($Anthocyanin_{mass}$, A), and leaf N content (N_{mass}, B), area-based leaf anthocyanin content ($Anthocyanin_{area}$, C), and leaf N content (N_{area}, D), F_v/F_m (E), and LED-specific leaf absorptance (ABS_{LED}, F) in leaves grown under high light at the south-faced outer-canopy (red circles, HL), intermediate light at north-faced outer-canopy (open rectangles, IL), and low light at north-faced inner-canopy (black closed triangles, LL) of an adult tree of fullmoon maple. Values are means $\pm$ SE (n=4). Insets enlarge seasonal changes in anthocyanins from the end of July to the middle of October. Leaves were sampled after the measurements of F_v/F_m on 27 Jul, 17 Aug, 7 Sep, 28 Sep, 5 Oct, 13 Oct, 19 Oct, 22 Oct, 26 Oct, and 29 Oct. Note: Leaf anthocyanins and N can be measured for the leaves sampled on 29 Oct, whereas F_v/F_m could not be measured, since fluorescence signals were too small because of almost no chlorophyll remained at that time (cf. Fig. 2).

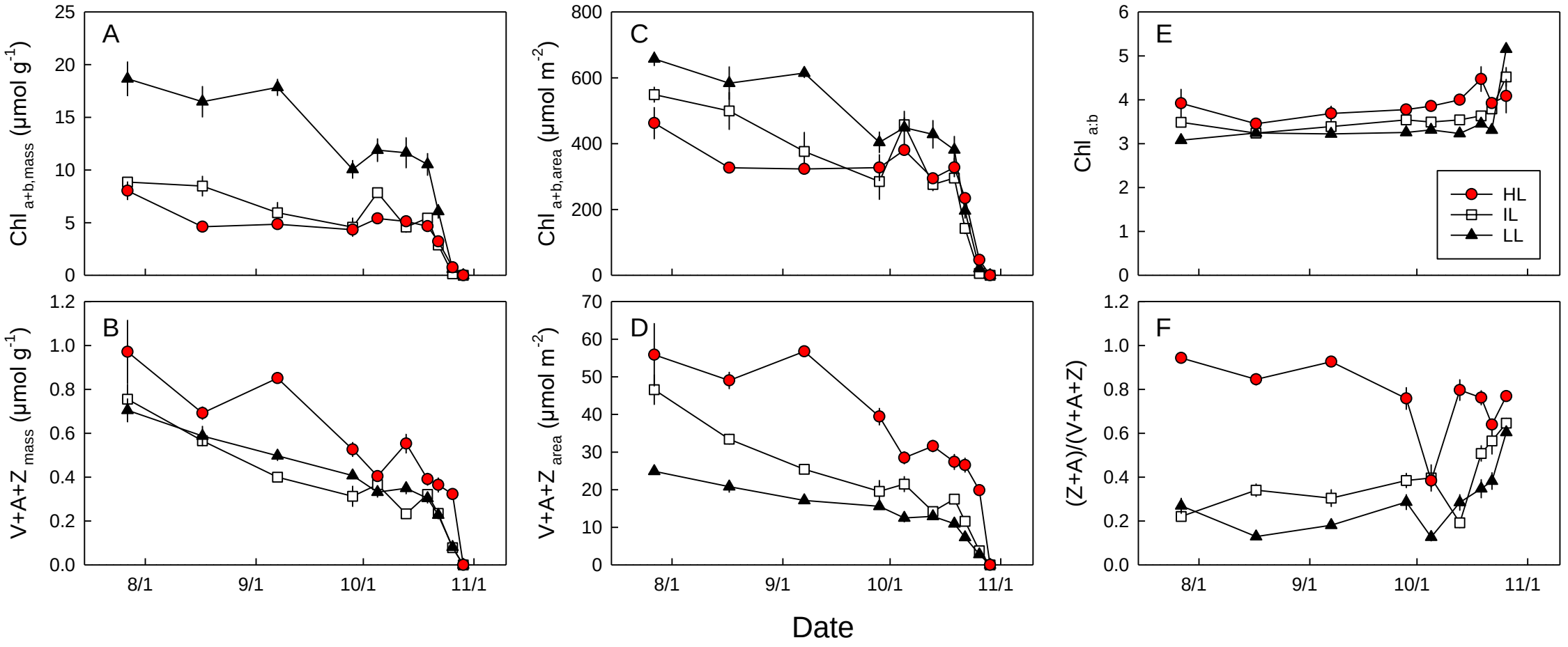

Figure 2. Seasonal changes in dry mass-based leaf chlorophyll content ($Chl_{a+b,mass}$, A), xanthophyll pigment pool size ($V+A+Z_{mass}$, B), area-based leaf chlorophyll content ($Chl_{a+b,area}$, C), xanthophyll pigment pool size ($V+A+Z_{area}$, D), the ratio of chlorophyll a to b ($Chl_{a:b}$, E), and conversion state of xanthophyll cycle [(Z+A)/(V+A+Z), F] in leaves grown at the south-faced outer-canopy (red circles, HL), north-faced outer-canopy (open rectangles, IL), and north-faced inner-canopy (black closed triangles, LL) of an adult tree of fullmoon maple. Values are means ± SE (n=4). Leaves were sampled on 27 Jul, 17 Aug, 7 Sep, 28 Sep, 5 Oct, 13 Oct, 19 Oct, 22 Oct, 26 Oct, and 29 Oct. Note: $Chl_{a:b}$ and (Z+A)/(V+A+Z) could not be calculated on 29 Oct, since the values of Chl_{a+b} and (V+A+Z) were not detectable (=0).

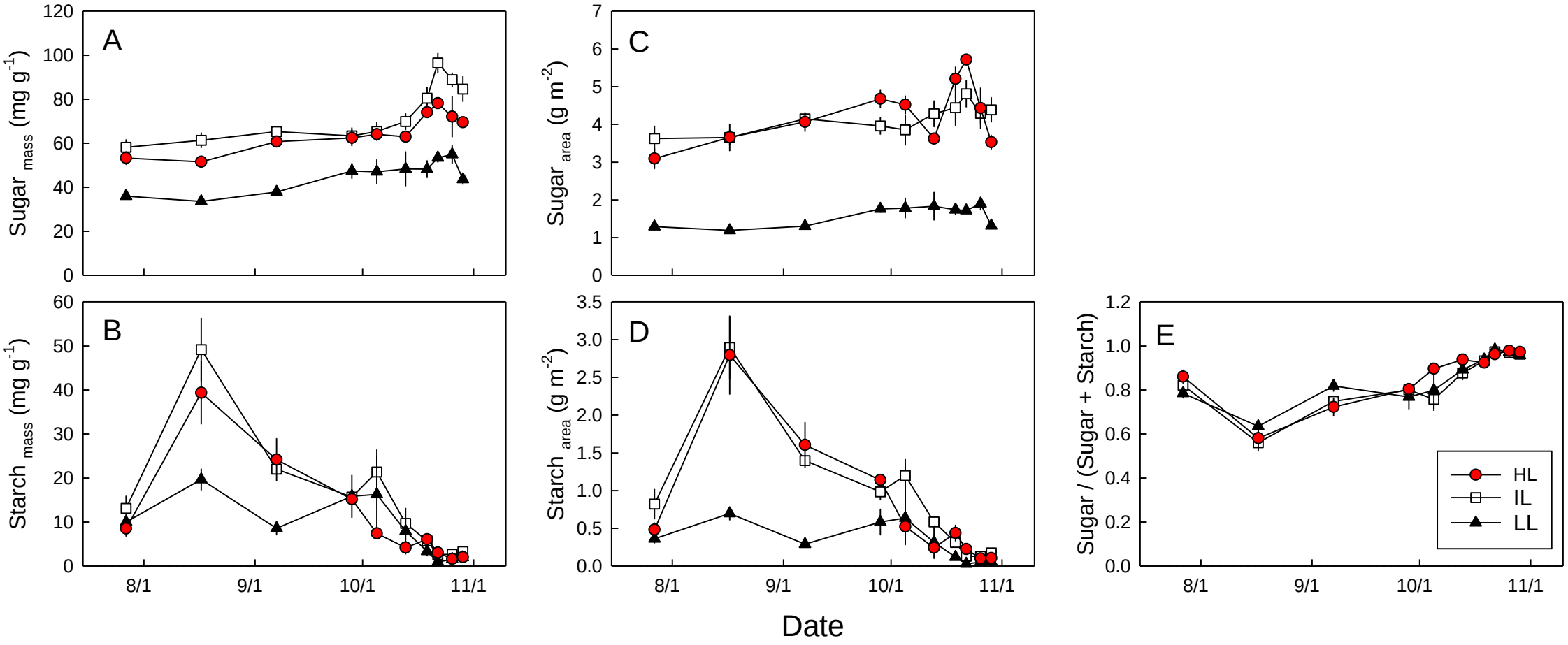

Figure 3. Seasonal changes in mass-based leaf sugar ($Sugar_{mass}$, A) and starch content ($Starch_{mass}$, B), area-based leaf sugar ($Sugar_{area}$, C) and starch content ($Starch_{area}$, D), and the ratio of leaf sugar to [sugar + starch] (Sugar/(Sugar + Starch), E) in leaves grown at the south-faced outer-canopy (red circles, HL), north-faced outer-canopy (open rectangles, IL), and north-faced inner-canopy (black closed triangles, LL) of an adult tree of fullmoon maple. Values are means ± SE (n=4). Leaves were sampled on 27 Jul, 17 Aug, 7 Sep, 28 Sep, 5 Oct, 13 Oct, 19 Oct, 22 Oct, 26 Oct, and 29 Oct.

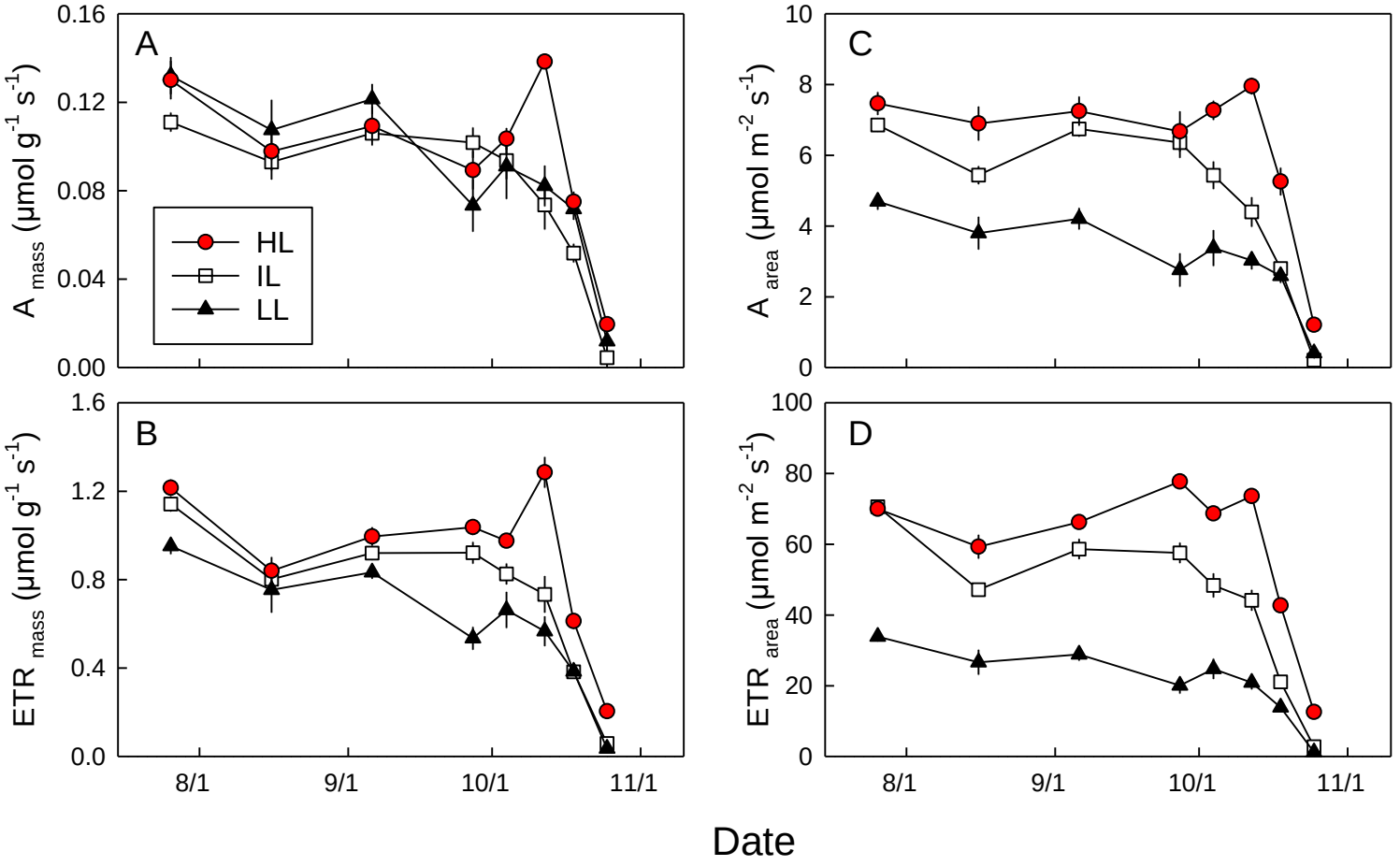

Figure 4. Seasonal changes in mass-based net photosynthetic rate (A_{mass}, A), electron transport rate (ETR_{mass}, B), area-based net photosynthetic rate (A_{area}, C), and electron transport rate (ETR_{area}, D) in leaves grown at the south-faced outer-canopy (red circles, HL), north-faced outer-canopy (open rectangles, IL), and north-faced inner-canopy (black closed triangles, LL) of an adult tree of fullmoon maple. Measurements were conducted under saturating light (1000 μmol m^{-2} s^{-1}) and optimal leaf temperature ranged from 20 to 25 ° C. Values are means ± SE (n=4). Measurements of gas exchange and chlorophyll fluorescence were conducted totally 8 times: 26 Jul, 16 Aug, 6 Sept, 27 Sept, 4 Oct, 12 Oct, 18 Oct, and 25 Oct in 2021.

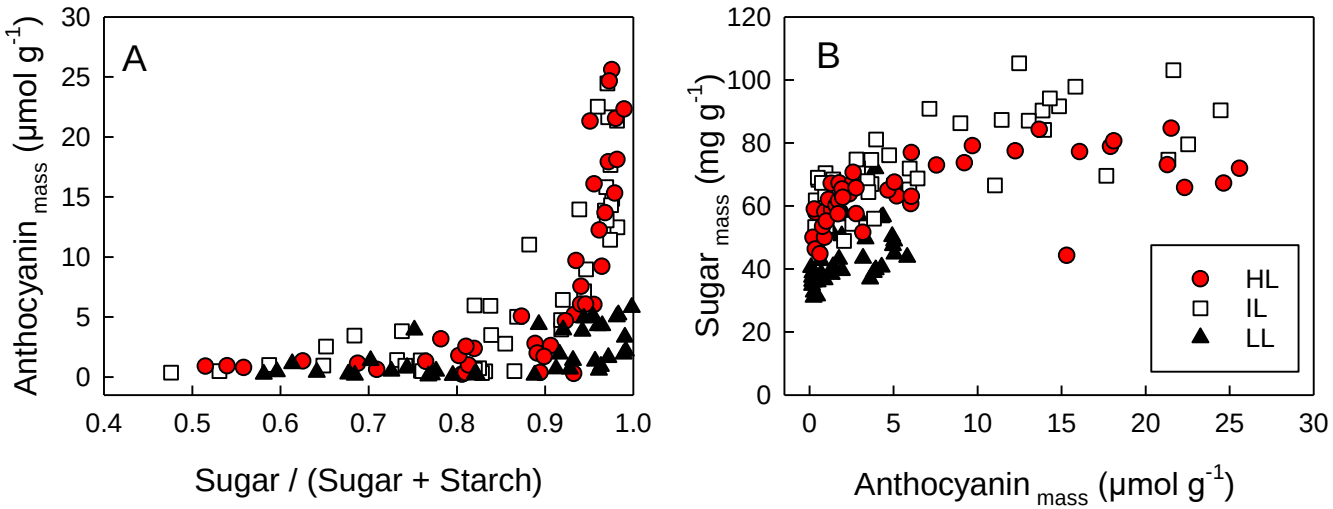

Figure 5. Relationships between the ratio of sugar to sugar plus starch [Sugar/(Sugar+Starch)] and $Anthocyanin_{mass}$ (A), and between $Anthocyanin_{mass}$ and $Sugar_{mass}$ (B), in leaves grown at the south-faced outer-canopy (red circles, HL), north-faced outer-canopy (open rectangles, IL), and north-faced inner-canopy (black closed triangle, LL) of an adult tree of fullmoon maple.

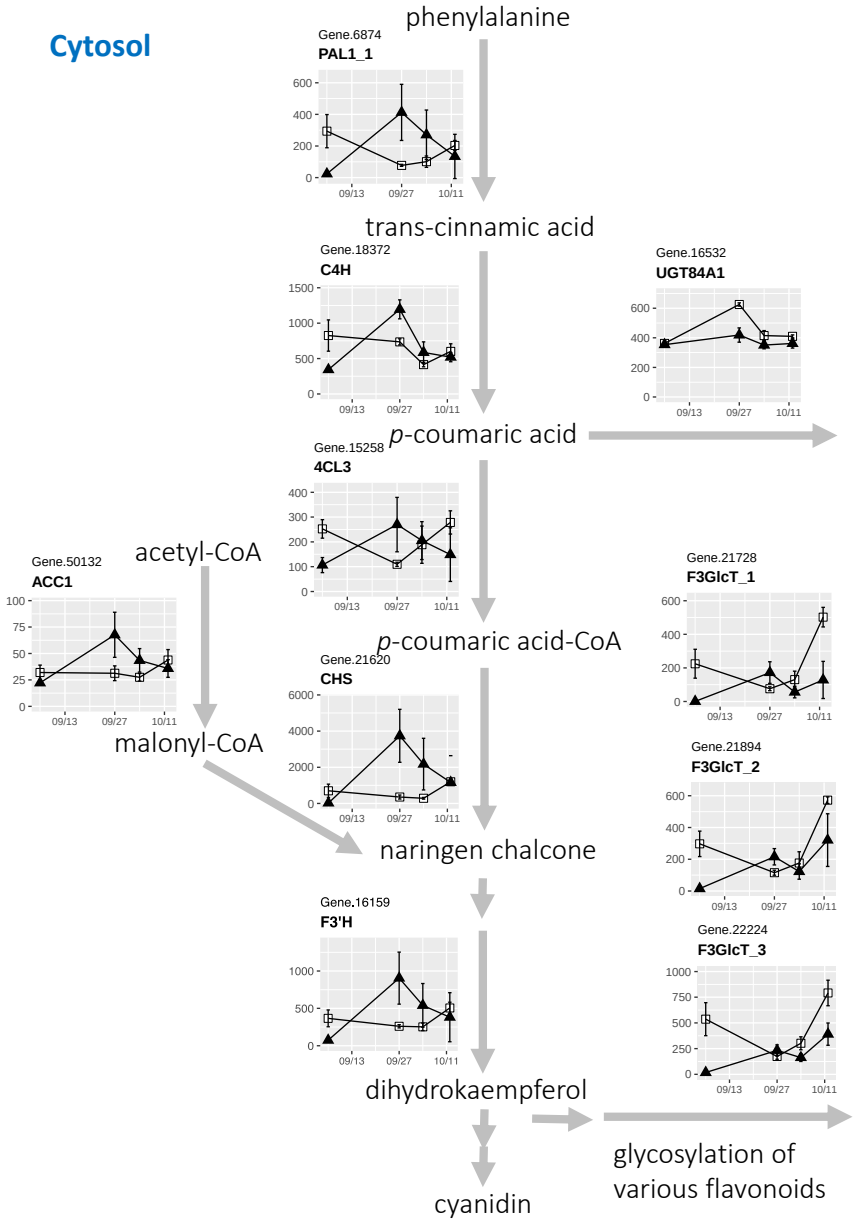

Figure 6. Expression of genes encoding key enzymes in flavonoid biosynthesis. The x-axes and the y-axes indicate dates and transcripts per million counts (TPM). Open rectangles indicate IL leaves, and black closed triangles LL leaves. Error bars indicate standard deviation (n = 3). Phenylalanine ammonia lyase (PAL) and accetyl-CoA carboxylase (ACC) are key enzymes to control the metabolic flow in anthocyanin synthesis (Saito *et al.*, 2013). Chalcone synthase (CHS) catalyzes the formation of naringenin chalcone, which is the committed step of all flavonoid compounds. This compound is further modified by several enzymes including flavonoid 3' hydroxylase (F3'H) to form cyanidin or related compounds. These compounds are further glycosylated by various glycosylases, including flavonoid 3-O-glucosyltransferase (F3GlcT; also called anthocyanin glycosyltranferase (Tohge *et al.*, 2005), and are stored in the vacuole.

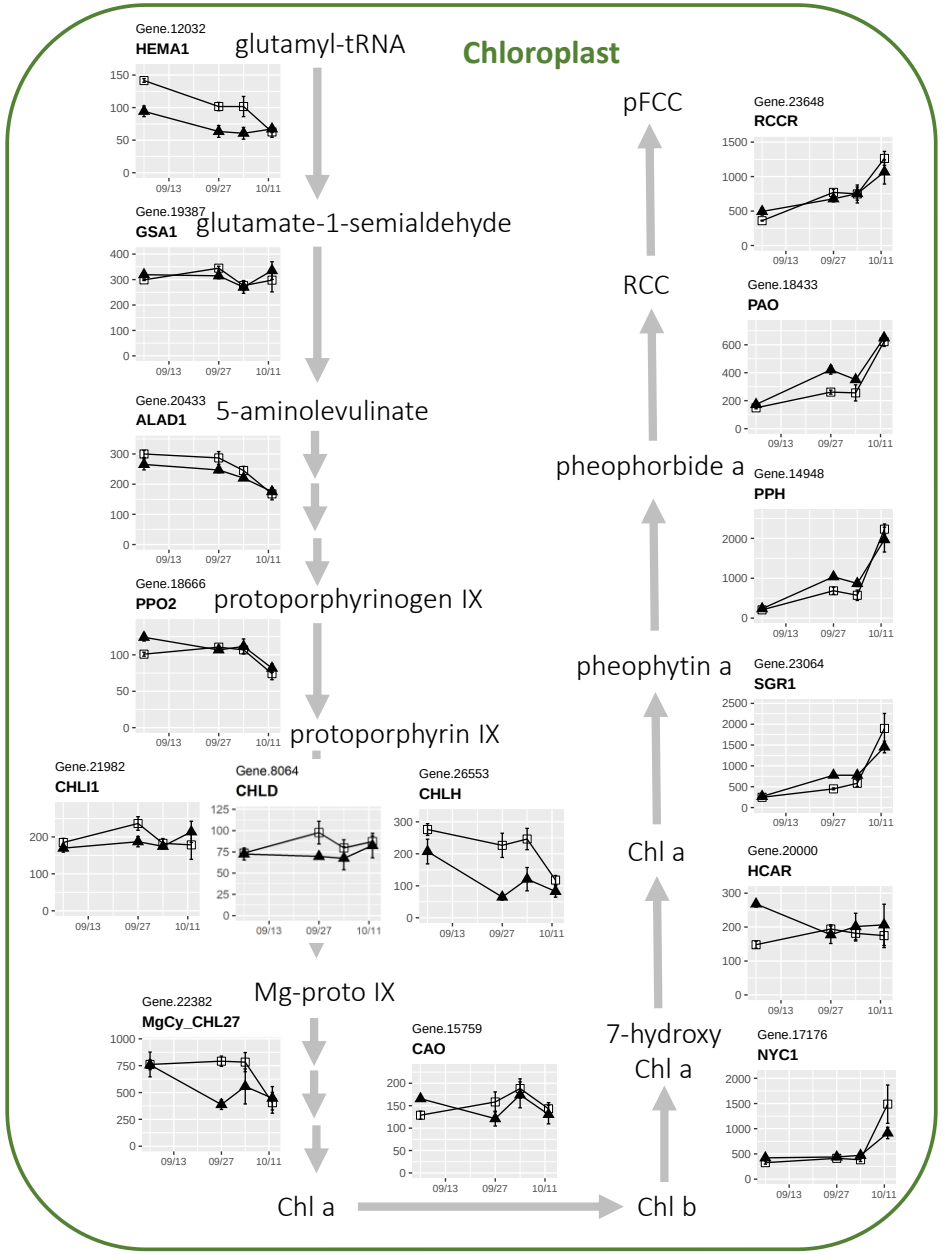

Figure 7. Expression of genes encoding key enzymes in chlorophyll biosynthesis and breakdown. The x-axes and the y-axes indicate dates and transcripts per million counts (TPM). Open rectangles indicate IL leaves, and black closed triangles LL leaves. Error bars indicate standard deviation (n = 3).

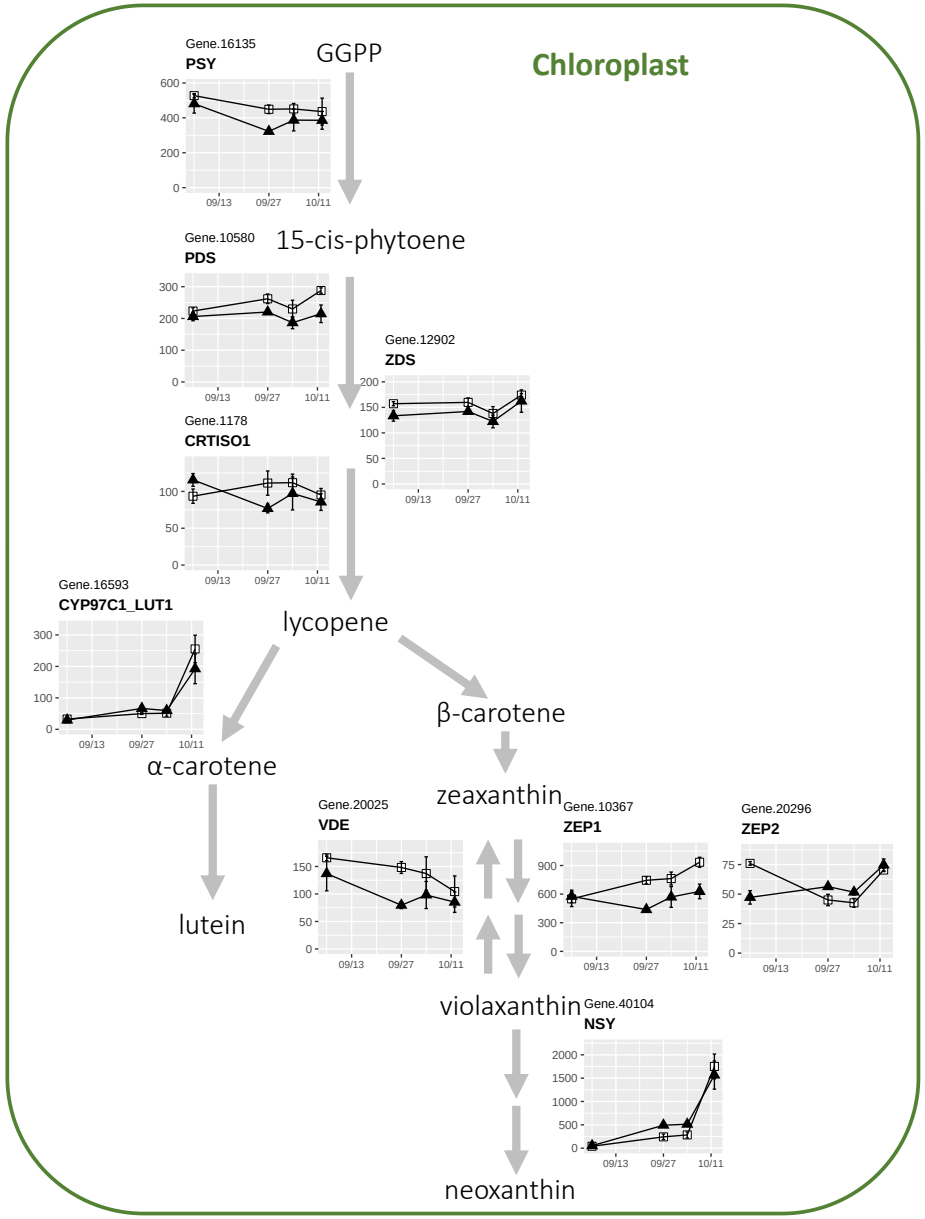

Figure 8. Expression of genes encoding key enzymes in carotenoid biosynthesis. The x-axes and the y-axes indicate dates and transcripts per million counts (TPM). Open rectangles indicate IL leaves, and black closed triangles LL leaves. Error bars indicate standard deviation (n = 3).

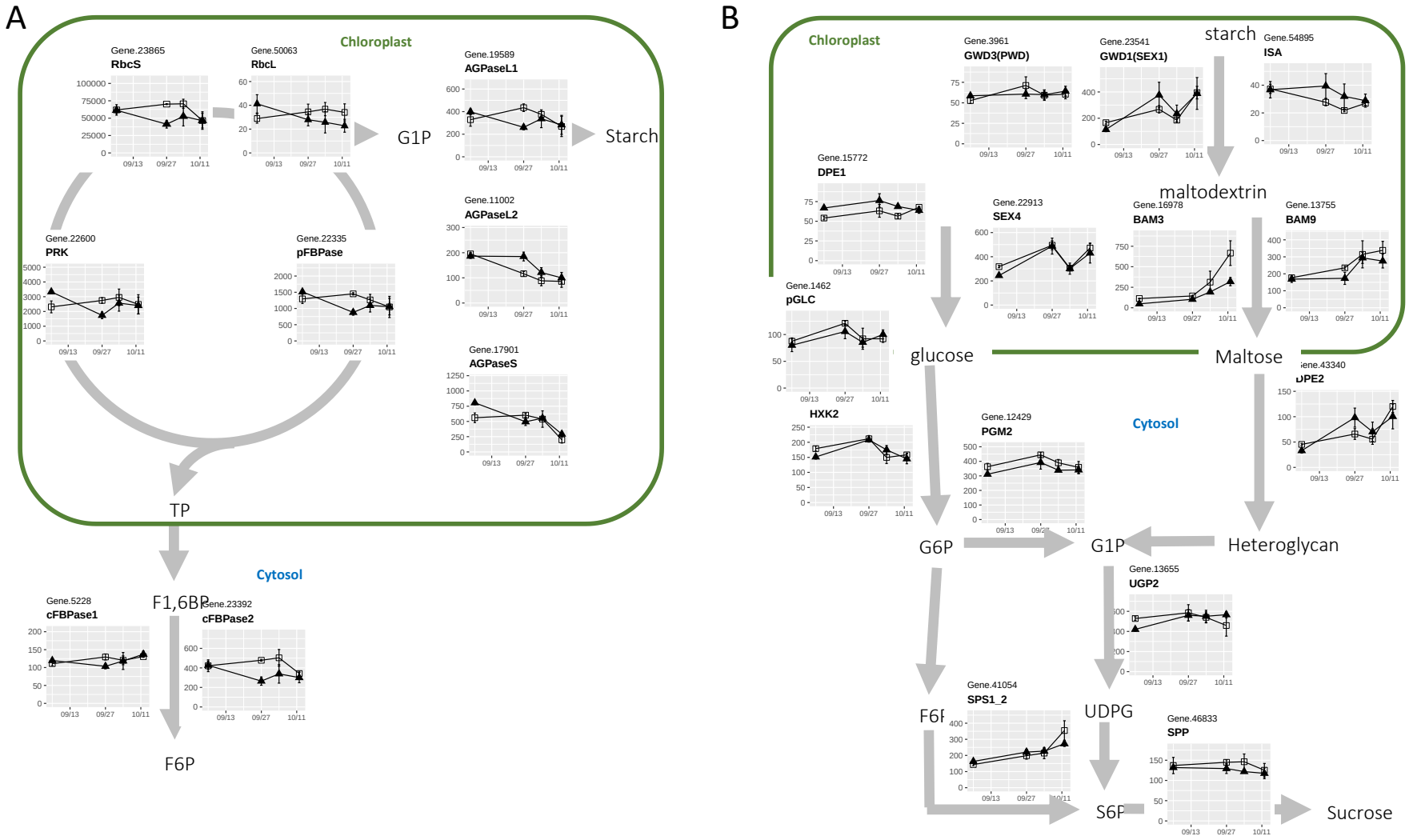

Figure 9. Expression of the genes encoding the key enzymes in carbohydrate metabolism, related to starch biosynthesis (A) and degradation (B). The X axes and the Y axes indicate dates and transcripts per million counts (TPM). Open rectangles indicate IL leaves, and black closed triangles LL leaves. Error bars indicate standard deviation (n = 3). TP: triose phosphate, G1P: glucose-1-phosphate, F1,6BP: fructose 1,6-bisphosphate. Note: RBCL is encoded by the plastid genome so that it was not expected to be detected after the purification of polyA mRNA for Iso-Seq analysis. Nevertheless, our Iso-Seq analysis detected a small amount of RbcL mRNA, which was possibly due to non-specific binding to the oligo-dT column.

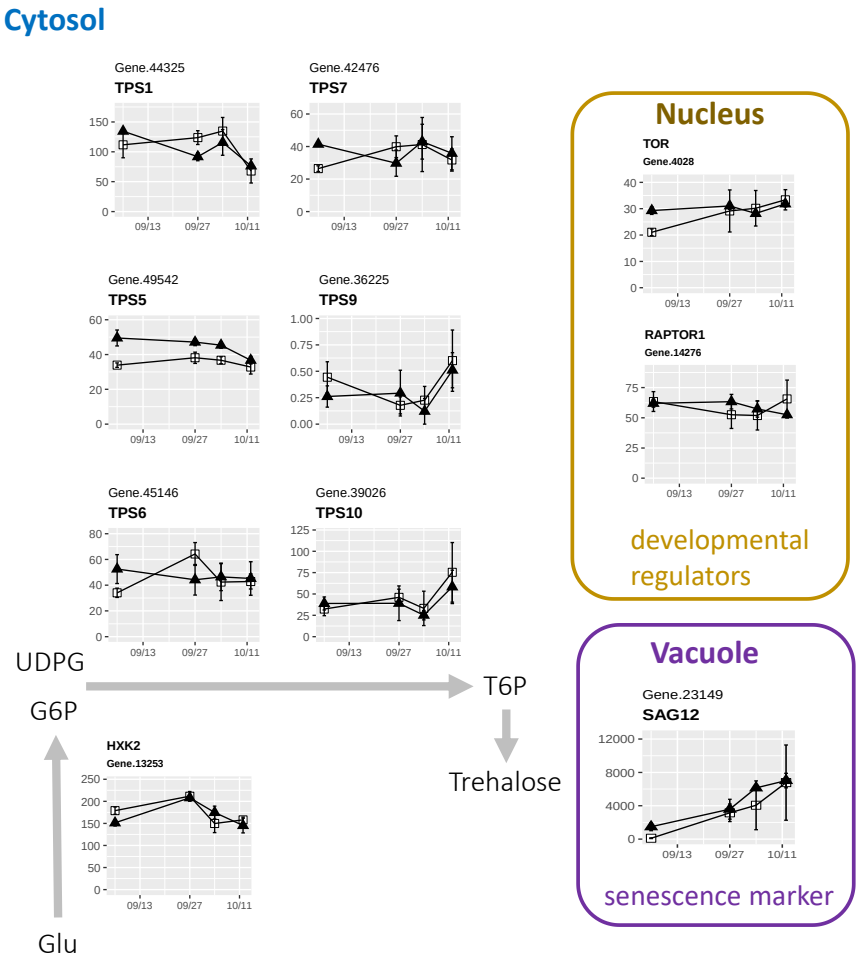

Figure 10. Expression of the genes related to the progression of leaf senescence. HXK denotes hexokinase. TOR is a protein kinase involved in the regulation of various developmental controls. RAPTOR is also involved in developmental controls by interacting with TOR. TPS denotes trehalose phosphate synthase. The numbers following TPS indicates the isoform numbers of the corresponding Arabidopsis homologs. An enzyme that catalyzes the formation of trehalose from trehalose-6-phosphate (T6P) was not detected in our Iso-Seq analysis. SAG12 (senescence-associated gene 12) encodes a vacuolar cysteine protease whose expression is well correlated with the progression of leaf senescence. The X axes and the Y axes indicate dates and transcripts per million counts (TPM). Open rectangles show gene expression under LL conditions, while black closed triangles indicate gene expression under IL conditions. Error bars indicate standard deviation. n = 3.

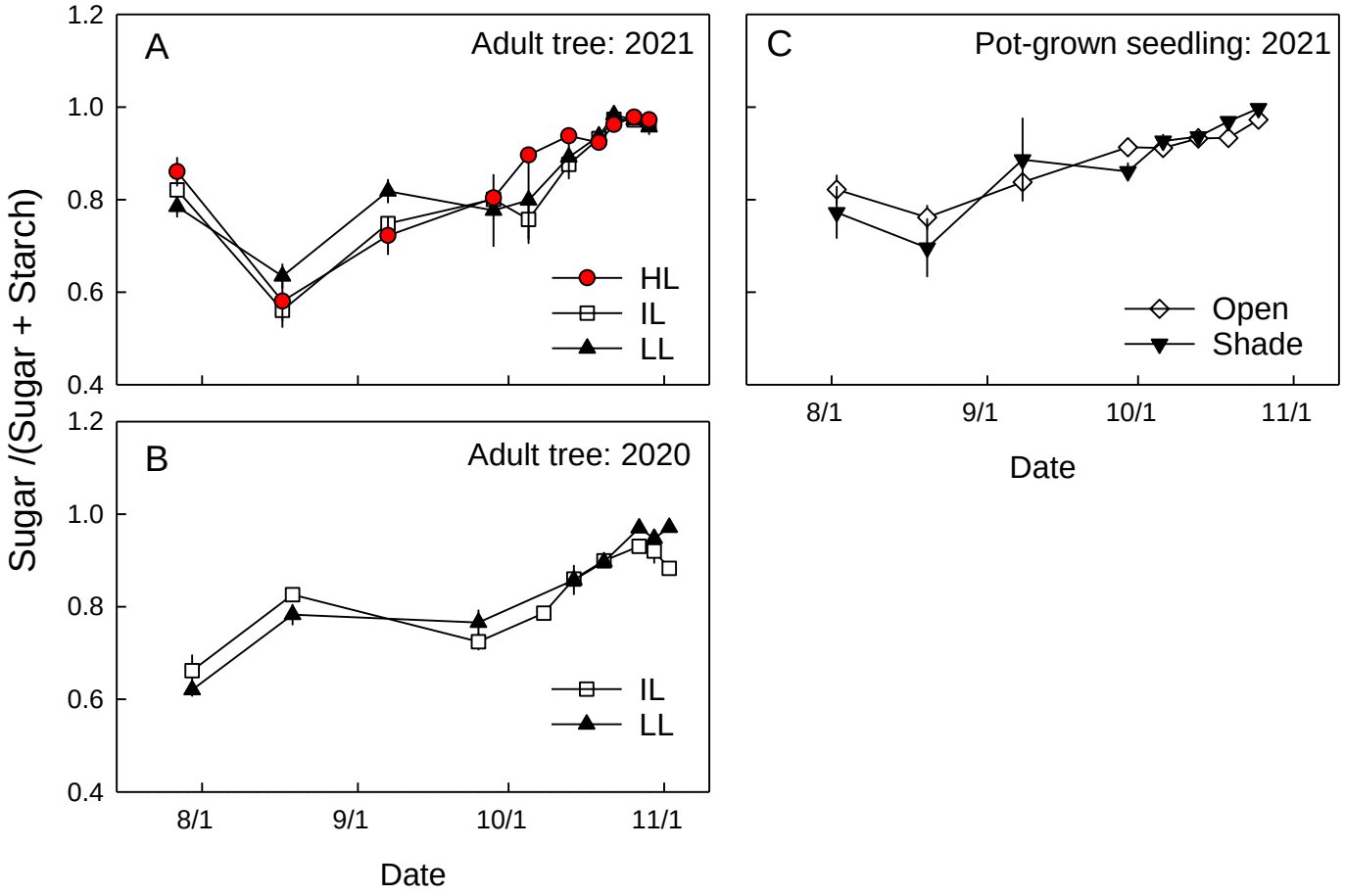

Figure 11. Seasonal changes in Sugar/(Sugar+Starch) in leaves of an adult tree of fullmoon maple grown under different light conditions in 2021 (cf. Fig. 4E) (A) and in 2020 (n=4 to 6) (cf. Fig. S9J) (B) in leaves grown at the south-faced outer-canopy (red circles, HL), north-faced outer-canopy (open rectangles, IL), and north-faced inner-canopy (black closed triangle, LL) of an adult tree of fullmoon maple, and that in pot-grown seedlings of fullmoon maple (4-year-old, ≈ 40 cm in shoot height) grown under open (open diamonds) (n=4) and shade: ≈13% of full sunlight (black closed triangles-down) in 2021 (n = 4 to 6) (C) (cf. Kitao et al. 2022). Error bars indicate standard error.